NATIONAL ADVISORY COMMITTEE FOR AERONAUTICS

TECHNICAL NOTE 4010

EXPERIMENTALLY DETERMINED NATURAL VIBRATION MODES OF SOME CANTILEVER-WING FLUTTER MODELS BY USING AN ACCELERATION METHOD

By Perry W. Hanson and W. J. Tuovila

Langley Aeronautical Laboratory
Langley Field, Va.

Washington
April 1957

NATIONAL ADVISORY COMMITTEE FOR AERONAUTICS

TECHNICAL NOTE 4010

EXPERIMENTALLY DETERMINED NATURAL VIBRATION MODES OF SOME CANTILEVER-WING FLUTTER MODELS BY USING AN ACCELERATION METHOD

By Perry W. Hanson and W. J. Tuovila

SUMMARY

Three-dimensional views are presented of the first three natural vibration mode shapes of ten cantilever-wing models. A table of normalized deflections at six spanwise and five chordwise stations is included for each mode. These mode shapes were measured by a rather unique experimental technique using grains of sand as accelerometers. The technique, which is particularly suited for measuring mode shapes of small wing models, is described and some of the difficulties likely to be encountered in applying the technique are discussed.

INTRODUCTION

In order to perform a modal-type flutter analysis of a wing, it is necessary to know the first few natural vibration modes. Several experimental methods can be used to determine them. A photographic technique is described in reference 1. Mirrors placed on the wing can be used to measure slopes from which deflections can be computed; accelerometers or micrometers which incorporate various sensing devices can be used to measure amplitudes directly. Mode shapes can also be calculated from measured influence coefficients. (See, for example, refs. 2 and 3.) These methods have disadvantages, however, when used on small wing models.

This paper describes a technique that is particularly suited for the measurement of mode shapes of small wing models. This technique is an extension of the technique described in reference 4 with the "chatter bar" replaced by sand. In addition to a description of the new technique, the first three mode shapes of ten cantilever-wing models are presented.

SYMBOLS

A	aspect ratio
b	wing semichord at root measured parallel to airstream
f_n	natural vibration frequency for the nth mode, cps
l	length of semispan of model measured normal to stream direction
t	thickness of wing
x	chordwise station, measured parallel to root chord from leading edge
y	spanwise station, measured perpendicular to root chord from the root
z	airfoil thickness ordinate, $\left(\frac{t}{4b}\right)100$
Λ	sweepback angle of quarter-chord line
λ	taper ratio

EXPERIMENTAL TECHNIQUE FOR DETERMINING NATURAL VIBRATION MODES

General Concept

A new technique, which may be termed "the 1 g method," is used in determining the natural vibration modes given in the present report. The technique is based on the principle that the acceleration of a particle vibrating in simple harmonic motion is the product of its amplitude and circular frequency squared. At any given frequency, therefore, particles having equal accelerations will also have equal amplitudes. An acceleration corresponding to that of gravity occurs when a particle placed on a vibrating wing just begins to rise from the surface.

In the 1 g method, the wing surface is sprinkled with sand and vibrated at one of its natural frequencies. A line, or lines, along which the acceleration is equal to gravity and the amplitude is, therefore, constant is obtained between regions of bouncing and stationary sand. By changing the magnitude of the exciting force the wing amplitudes are changed and the location of the 1 g line or lines is changed. This is illustrated in figure 1 which shows a hypothetical wing vibrating in first bending at three discrete amplitudes. The abscissa is the wing

semispan and the ordinate is the acceleration. The cross-hatching on each curve represents regions where the sand is bouncing (accelerations greater than that of gravity). The boundaries between regions of bouncing and stationary sand are shown at spanwise locations a, b, and c. For each of the three wing amplitudes shown in figure 1, the strain is measured at the wing root. It is assumed that the wing amplitude varies linearly with root strain and that the relative distribution of amplitude (mode shape) is independent of absolute amplitude. The following analysis shows how the root strains are used to convert the 1 g lines into "contour lines" that define the wing mode shape. (Refer to figure 1.)

Let δ_{x_n} be deflection at semispan location x for wing amplitude n and σ_n be strain associated with amplitude n, and its corresponding 1 g line. Then,

$$\frac{\delta_{a_3}}{\delta_{a_1}} = \frac{\sigma_3}{\sigma_1} \quad \text{or} \quad \delta_{a_3} = \frac{1}{\sigma_1}\left(\sigma_3 \delta_{a_1}\right)$$

If similar relations are written for the other deflections, based on the arbitrary wing amplitude 3, at spanwise stations b and c, the quantity in the parenthesis is seen to be a constant. Since the deflections defining the mode shape are relative, this constant may be taken to be 1. The 1 g lines thus become contour lines with amplitudes equal to the reciprocal of the strain associated with the line. By varying the magnitude of the wing exciting force in six or seven steps, a sufficient number of contour lines are located to define the mode shape.

Equipment

The wing models were cantilevered from a large backstop and were excited acoustically by a public address system loudspeaker with the horn removed. The loudspeaker was driven by a wide-range oscillator through a direct-coupled amplifier. The signal from strain gages on the wing root was fed through an amplifier to an electronic voltmeter placed beside the wing. A modified aerial camera mounted on the backstop above the wing was used to photograph the sand pattern and the voltmeter reading for each contour line. The sand used was washed and throughly dried to minimize sticking to the wing.

Technique

After clamping the model to the backstop, it was carefully cleaned to remove dirt and fingerprints which might cause the sand to stick to the wing. The loudspeaker unit was placed beneath the wing and the output

frequency varied until reasonance in the desired natural mode was indicated by a maximum deflection of the voltmeter needle.

The loudspeaker was turned off and sand was sprinkled lightly over the surface of the model. The volume of the loudspeaker was slowly increased until the sand just started moving somewhere on the wing, usually at the tip or along one of the edges, depending on the mode. The camera shutter was opened for a time exposure to record the movement of the sand and the corresponding root strain indicated on the dial of the electronic voltmeter. Also recorded in the photograph were the wing identification and numbers indicating the attenuation setting of the strain-gage amplifier. The volume of the loudspeaker was further increased to move the contour line to a different position on the wing and another photograph was taken. The process was repeated in steps until all the sand on the wing was moving except along the node lines. Usually, six or seven photographs were sufficient to give a good spacing of the contour lines from the wing tip or edges to the node lines.

Interpretation of Data

The raw data are a series of photographs, each showing regions where the sand is blurred (moving) and sharp (stationary) and a meter reading and amplifier attenuation showing the corresponding root strain. A sample photograph is shown in figure 2. Here the wing is vibrating in the third mode and two regions of stationary sand, A and C, and two regions of moving sand, B and D may be seen. Regions A and C are vibrating with an acceleration less than that of gravity, and regions B and D with an acceleration greater than that of gravity. The lines separating these regions are vibrating with an acceleration equal to that of gravity and therefore are lines of equal amplitude. The meter reading multiplied by the amplifier attenuation, 30, gives the relative strain at the root associated with these particular lines. The numbers and letters at the top of the photograph are wing, mode, and frequency identifications.

Lines separating the regions of moving and stationary sand were drawn on each photograph and a composite drawing of the wing was made showing the locations of the various lines of equal amplitude. The reciprocal of the root strain for each of these lines was noted on the composite drawing. These numbers indicate the relative deflection of the wing along that particular line. A sample composite drawing is shown in figure 3. The whole numbers beside each line identify the photograph from which the lines were obtained and the fractional numbers indicate the relative deflection.

Each wing was divided into six spanwise stations at 0.1, 0.3, 0.5, 0.7, 0.9, and 1.0 semispan, and five chordwise stations at 0, 0.25, 0.50, 0.75, and 1.00 chord, as shown in figure 3. A plot was made of relative

amplitude of deflection against semispan distance y/l at each of the five chordwise stations. Another plot was made of relative amplitude of deflection against chord, $x/2b$, at each of the six semispan stations. After fairing each of these plots by cross reference to the other, the values of the relative deflections at the intersections of the various spanwise and chordwise stations were normalized on the maximum deflection and arranged in tabular form. Examples of such plots are shown in figures 4 and 5. A three-dimensional composite view, as shown in figure 6, was chosen to illustrate the mode shapes because of the complexity of some of the modes.

Limitations

The acceleration technique described in this paper has certain inherent limitations.

The surface of the wing must be nearly horizontal so that sand particles do not roll and thereby give the impression of bouncing. This condition is encountered at the leading edge of most airfoil shapes; however, with a little experience, allowance for this effect can be made in the interpretation of the results. A thick symmetrical double-wedge section, however, might present this problem over the entire wing surface. Low frequency modes are difficult to measure by using this technique due to the large amplitudes required to obtain accelerations equal to gravity.

Models that are very light in weight and also very lowly damped (having sharply tuned reasonances) present difficulties because of the rapid increase in amplitude near the resonant frequency. The sand that is sprinkled on the wing increases the mass of the wing enough to cause its frequency to shift slightly and thereby change its amplitude considerably. This condition makes control of the wing amplitude difficult as sand bounces off. Control of the amplitude can be maintained by adjusting the shaker frequency and output.

EXPERIMENTAL VIBRATION MODES OF SEVERAL FLUTTER MODELS

Description of Models

A complete description of the test models is presented in figure 7. In order that thickness distribution of the models may be readily available, the ordinates of the section shapes, except for the flat plate models, are presented in table I.

The models were sprayed lightly with a flat black paint to serve as a background for the white sand. Electrical resistance strain gages were mounted at the root.

Results and Discussion

The first three natural vibration modes and frequencies are shown in figures 8 to 17. The modes are presented in perspective, looking from the root to the tip with the leading edge on the viewer's right. The wing semispans have been foreshortened slightly as an aid in perspective, and the wing deflections have been normalized on the maximum deflection.

The vibration modes, as drawn, provide a quick qualitative representation of the manner in which the vibrating wing is deflecting. For a more detailed analysis of the vibration modes, tables of the normalized deflections at the 0.1, 0.3, 0.5, 0.7, 0.9, and 1.0 semispan, and the 0, 0.25, 0.50, 0.75, and 1.00 chord stations are presented with each drawing.

The first three mode shapes and frequencies for a cantilevered rectangular 2- by 5- by 0.064-inch magnesium plate were measured and are presented in figure 18. Also presented in the figure are theoretically obtained mode shapes and frequencies. First torsion modes were calculated by means of the plate theory of reference 5 (using the solution of eq. (43)) and also by means of elementary torsion theory. (See, for example, ref. 3.) Elementary beam theory was used to calculate the bending modes.

CONCLUDING REMARKS

A unique acceleration technique for measuring the natural vibration mode shapes of small wing models is described. The first three natural vibration mode shapes are presented for ten cantilever-wing models.

Langley Aeronautical Laboratory,
National Advisory Committee for Aeronautics,
Langley Field, Va., December 6, 1956.

REFERENCES

1. Herr, Robert W.: Preliminary Experimental Investigation of Flutter Characteristics of M and W Wings. NACA RM L51E31, 1951.

2. Bisplinghoff, Raymond L., Ashley, Holt, and Halfman, Robert L.: Aeroelasticity. Addison-Wesley Pub. Co., Inc. (Cambridge, Mass.), c.1955.

3. Scanlan, Robert H., and Rosenbaum, Robert: Introduction to the Study of Aircraft Vibration and Flutter. The Macmillan Co., 1951.

4. Bragg, William: An Instrument for Measuring Small Amplitudes of Vibration. Jour. Sci. Instr., vol. VI, no 6, June 1929, pp. 196-197.

5. Reissner, Eric, and Stein, Manuel: Torsion and Transverse Bending of Cantilever Plates. NACA TN 2369, 1951.

TABLE I

NACA 65A AIRFOIL ORDINATES FOR $t/2b = 0.020$ and $t/2b = 0.040$

$100\left(\frac{x}{2b}\right)$	NACA 65A002 ±z	NACA 65A004 ±z
0	0	0
.5	.156	.311
.75	.190	.378
1.25	.242	.481
2.5	.329	.656
5.0	.439	.877
7.5	.531	1.062
10.0	.608	1.216
15	.731	1.463
20	.824	1.649
25	.895	1.790
30	.947	1.894
35	.981	1.962
40	.998	1.996
45	.997	1.996
50	.977	1.952
55	.936	1.867
60	.874	1.742
65	.796	1.584
70	.704	1.400
75	.601	1.193
80	.488	.966
85	.369	.728
90	.247	.490
95	.126	.249
100	.005	.009
Leading-edge radius . .	0.0255	0.102
Trailing-edge radius . .	0.0045	0.010

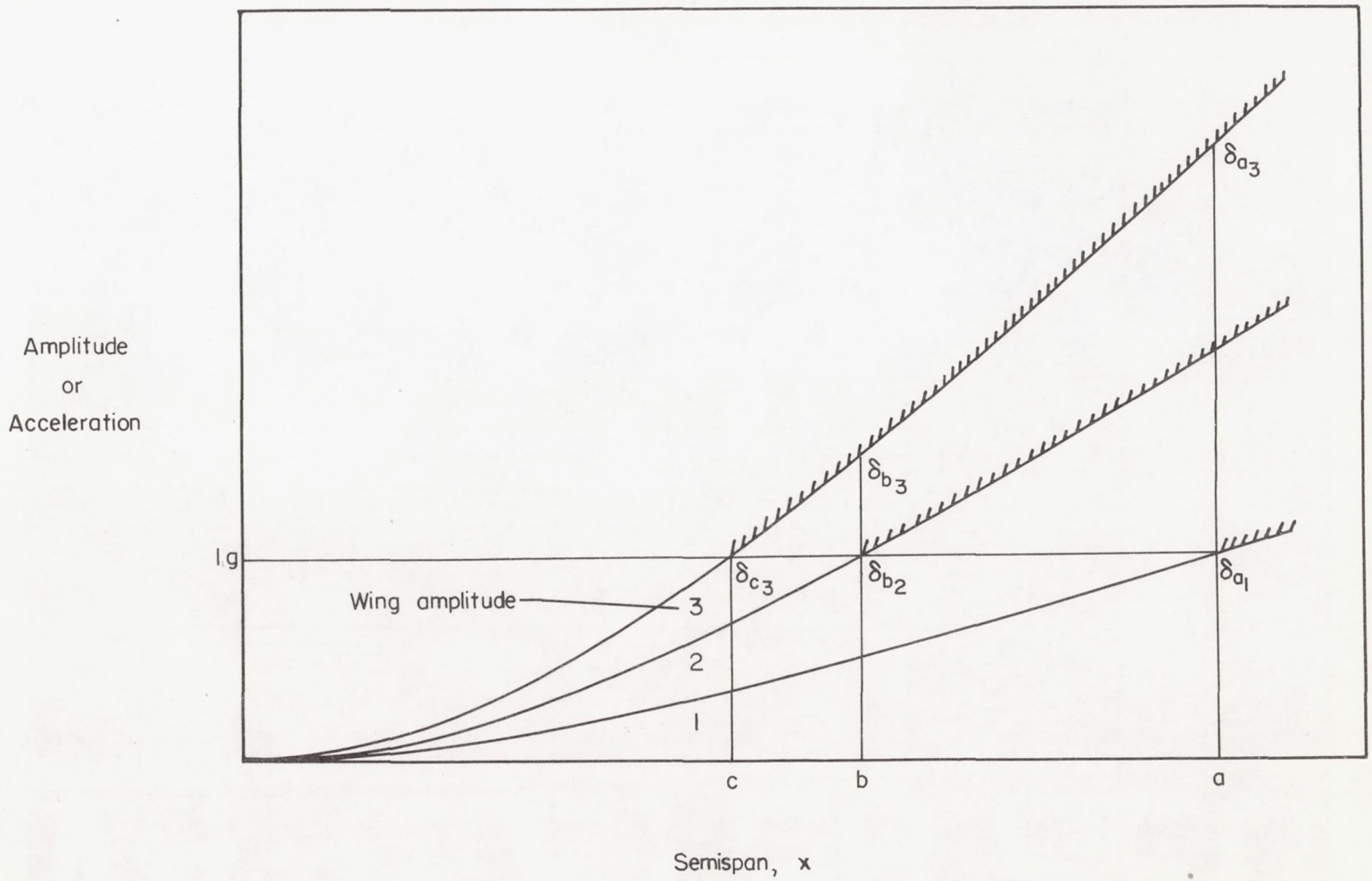

Figure 1.- Illustration of the relation of the 1 g lines to wing amplitudes.

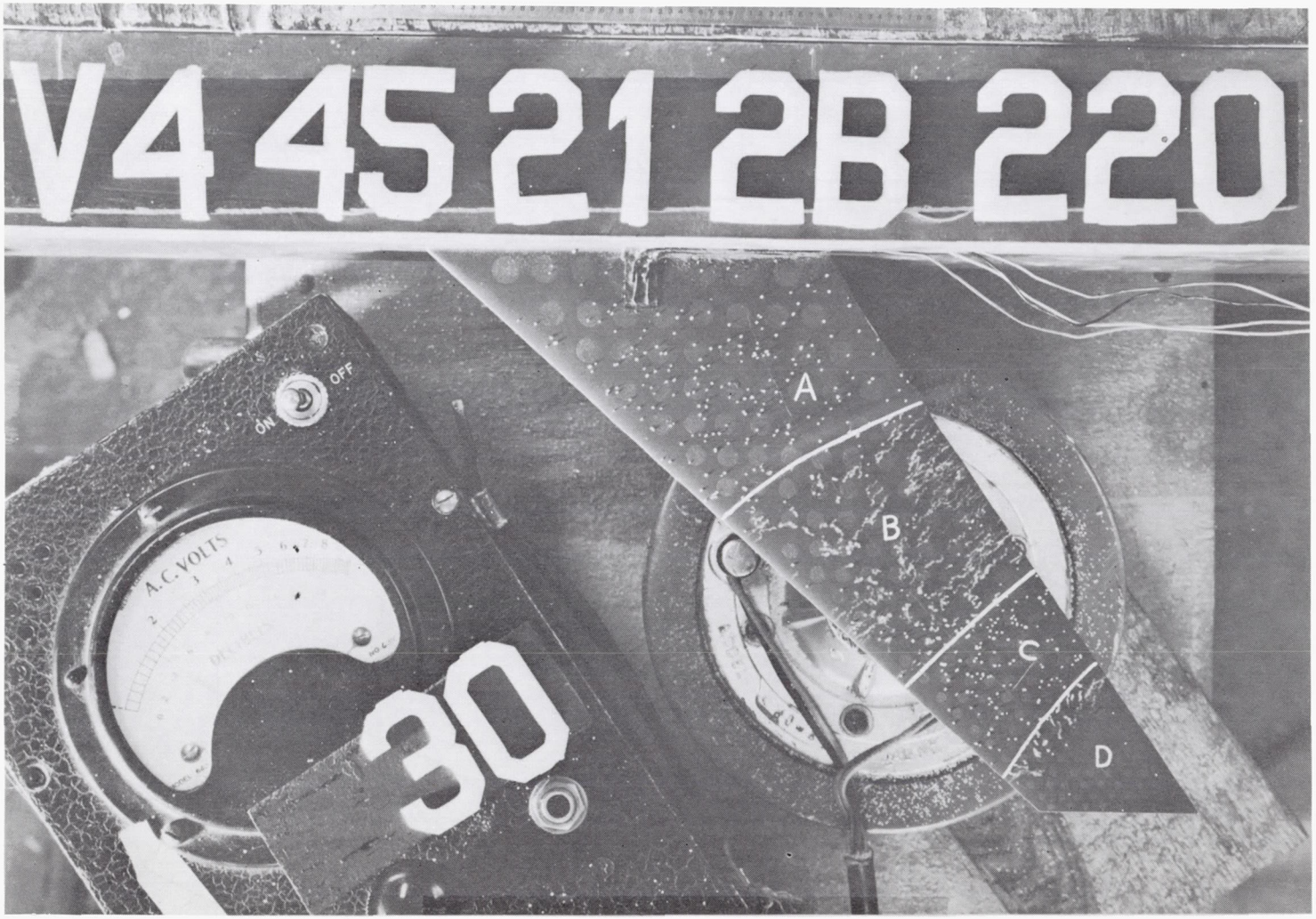

L-95907

Figure 2.- Sample photograph showing how the regions of moving and stationary sand indicate contour lines.

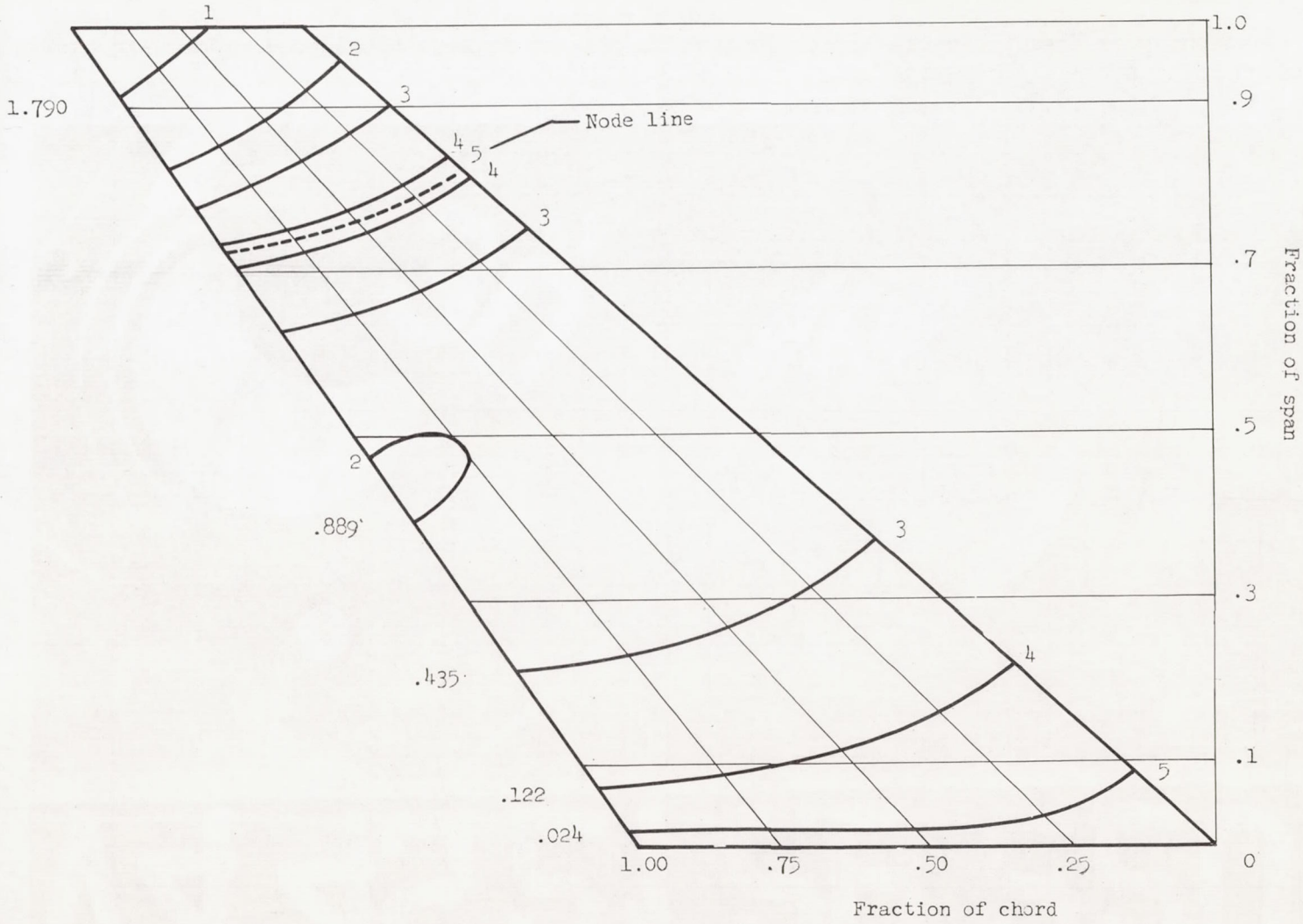

Figure 3.- Sample of a composite drawing of a 45° swept-tapered wing vibrating in the third mode showing the contour lines.

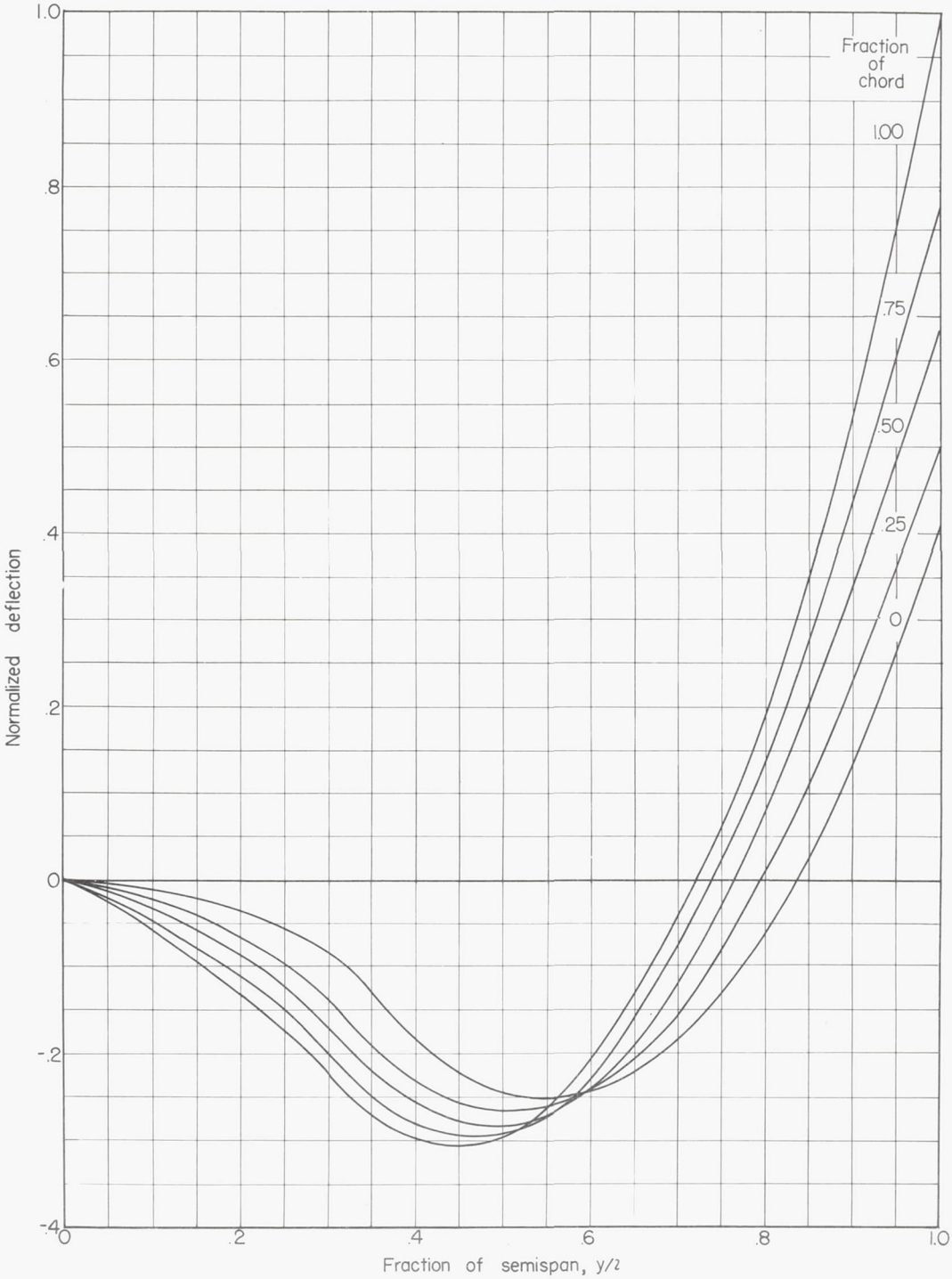

Figure 4.- Normalized deflection of a 45° swept-tapered wing plotted against semispan for five chordwise locations.

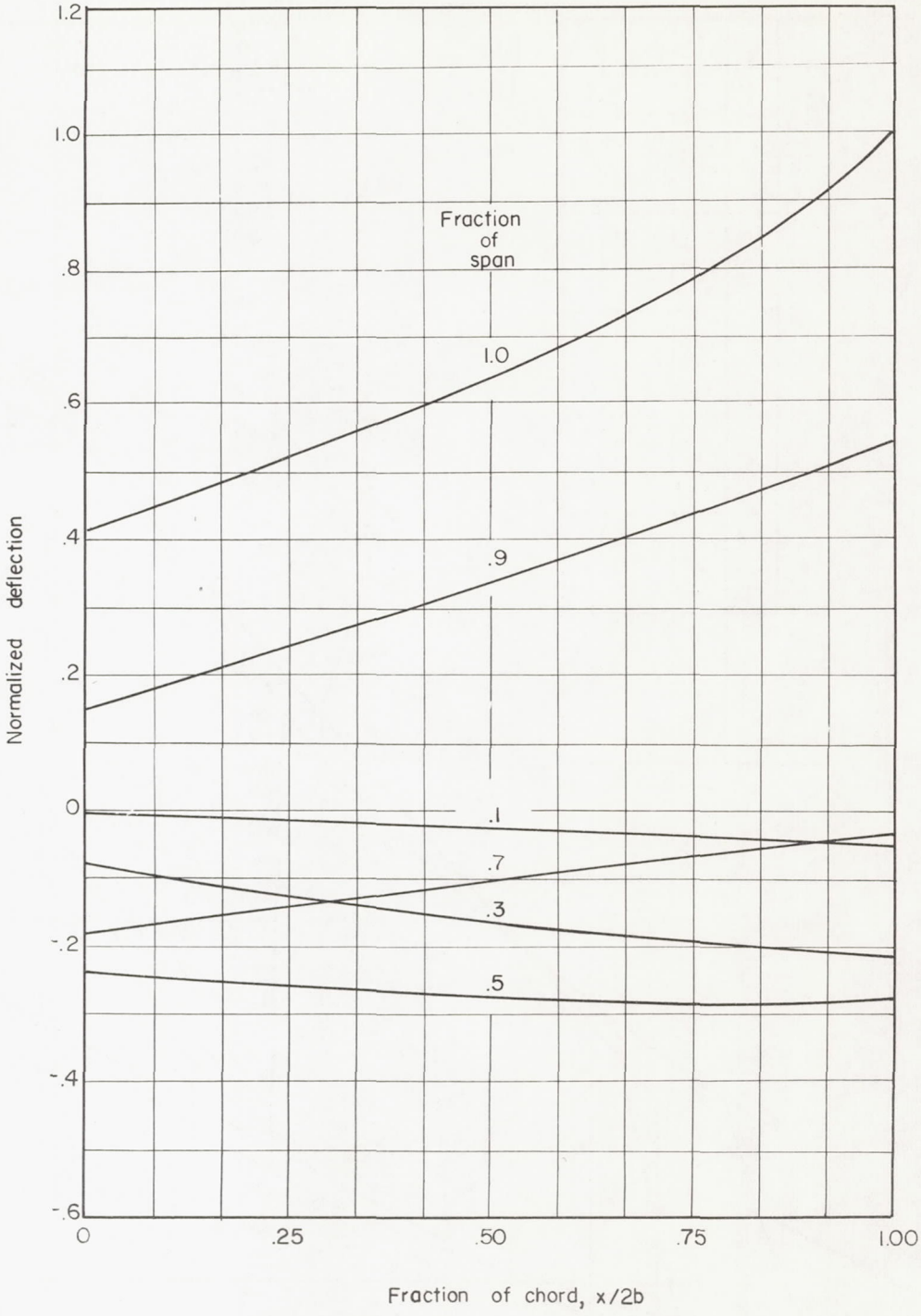

Figure 5.- Normalized deflection of a 45° swept-tapered wing plotted against chord for six spanwise locations.

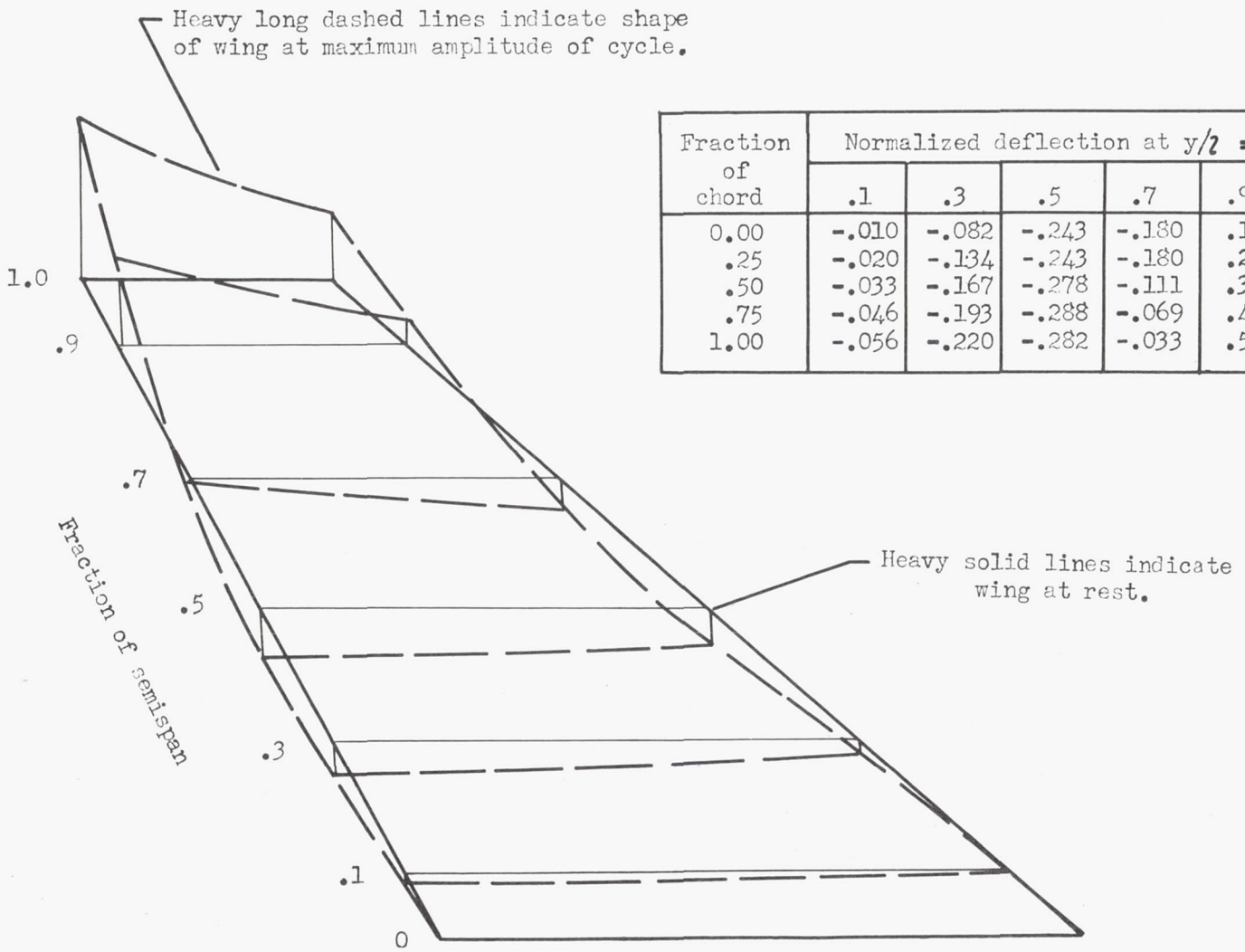

Fraction of chord	Normalized deflection at y/ℓ =					
	.1	.3	.5	.7	.9	1.0
0.00	-.010	-.082	-.243	-.180	.147	.416
.25	-.020	-.134	-.243	-.180	.239	.518
.50	-.033	-.167	-.278	-.111	.338	.639
.75	-.046	-.193	-.288	-.069	.436	.787
1.00	-.056	-.220	-.282	-.033	.541	1.000

Figure 6.- Third natural vibration mode. f_3 = 220 cycles per second.

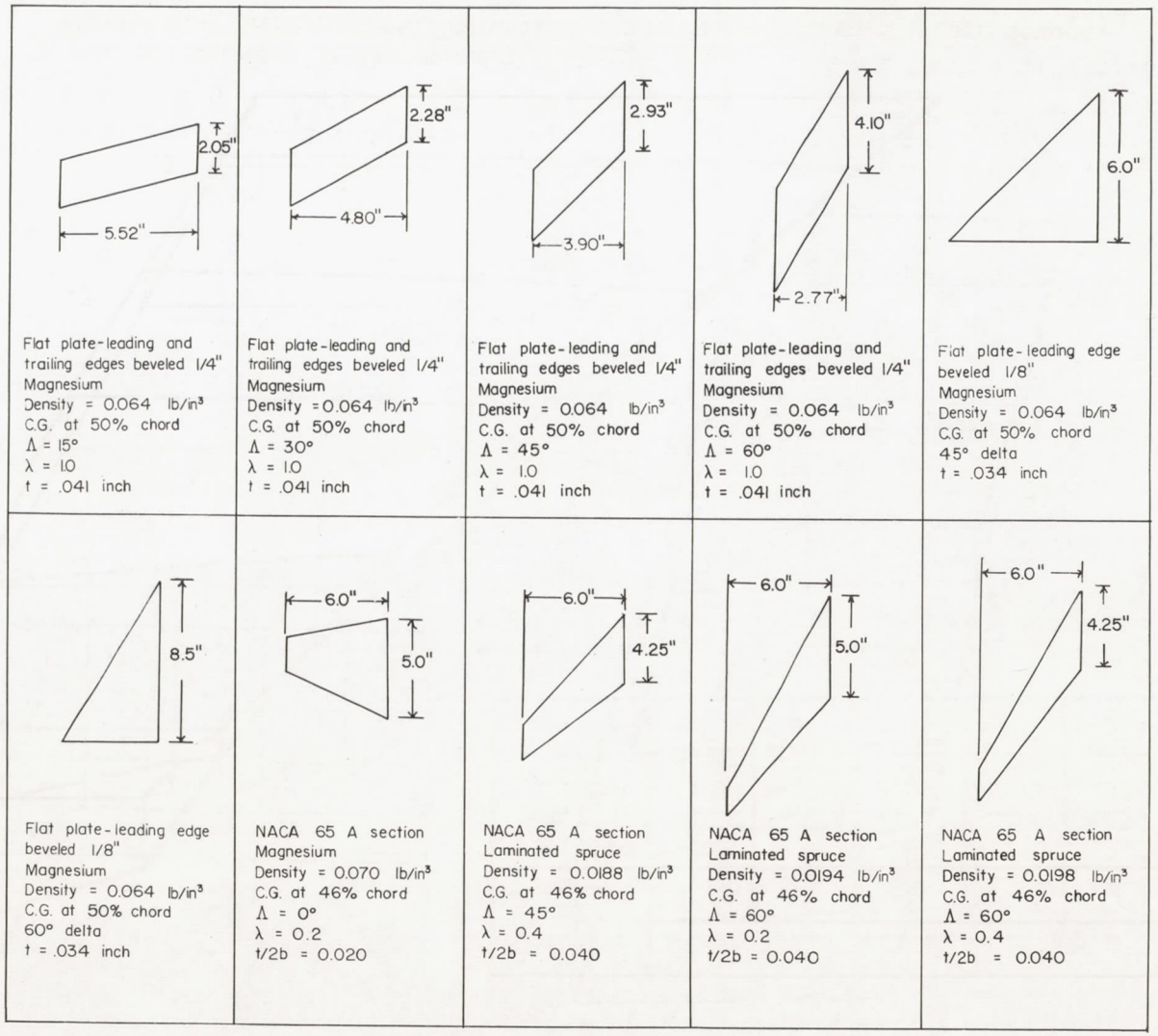

Figure 7.- Dimensions, density, and center-of-gravity location of wing models. Sweep angles are measured from 0.25 chord.

Fraction of chord	Normalized deflection at y/ℓ =					
	.1	.3	.5	.7	.9	1.0
0.00	.039	.160	.316	.547	.800	.935
.25	.043	.175	.338	.569	.817	.952
.50	.048	.185	.360	.589	.840	.966
.75	.053	.200	.383	.608	.856	.983
1.00	.056	.225	.406	.631	.875	1.000

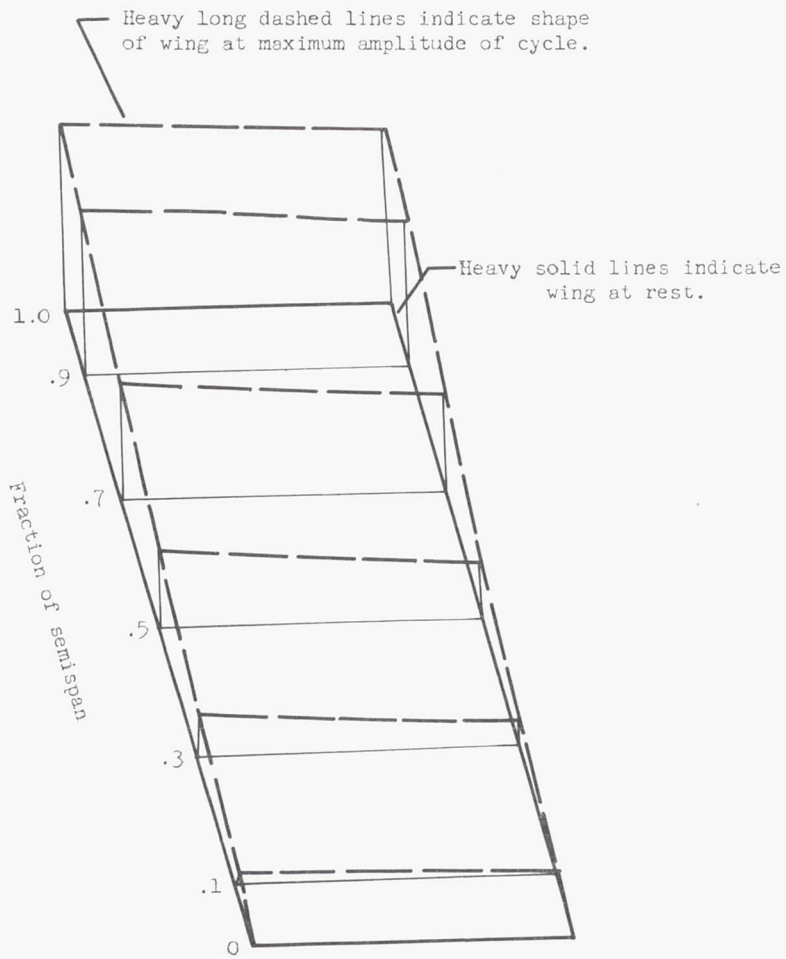

(a) First natural vibration mode; f_1 = 35 cycles per second.

Figure 8.- Natural vibration modes for magnesium flat-plate model. $\Lambda = 15^{\circ}$; $\lambda = 1.0$; $t/2b = 0.020$; $A = 5.35$.

Fraction of chord	Normalized deflection at y/ℓ =					
	.1	.3	.5	.7	.9	1.0
0.00	-.088	-.361	-.579	-.485	-.207	-.055
.25	-.080	-.289	-.407	-.297	-.008	.117
.50	-.069	-.210	-.260	-.106	.180	.310
.75	-.044	-.135	-.120	.100	.386	.524
1.00	-.014	-.062	.014	.331	.758	1.000

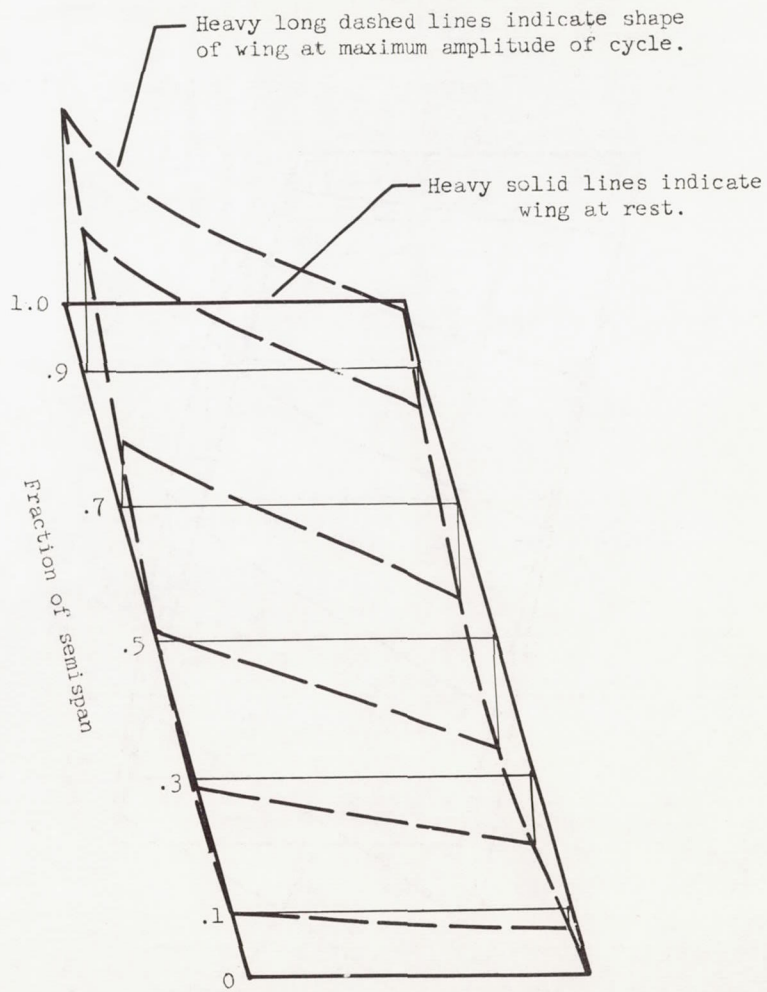

(b) Second natural vibration mode; f_2 = 205 cycles per second.

Figure 8.- Continued.

Fraction of chord	Normalized deflection at y/ℓ =					
	.1	.3	.5	.7	.9	1.0
0.00	.099	.106	.162	.401	.788	1.000
.25	.021	-.035	-.021	.176	.472	.654
.50	-.042	-.190	-.225	-.085	.190	.352
.75	-.099	-.345	-.451	-.338	-.099	.085
1.00	-.155	-.556	-.831	-.746	-.373	-.162

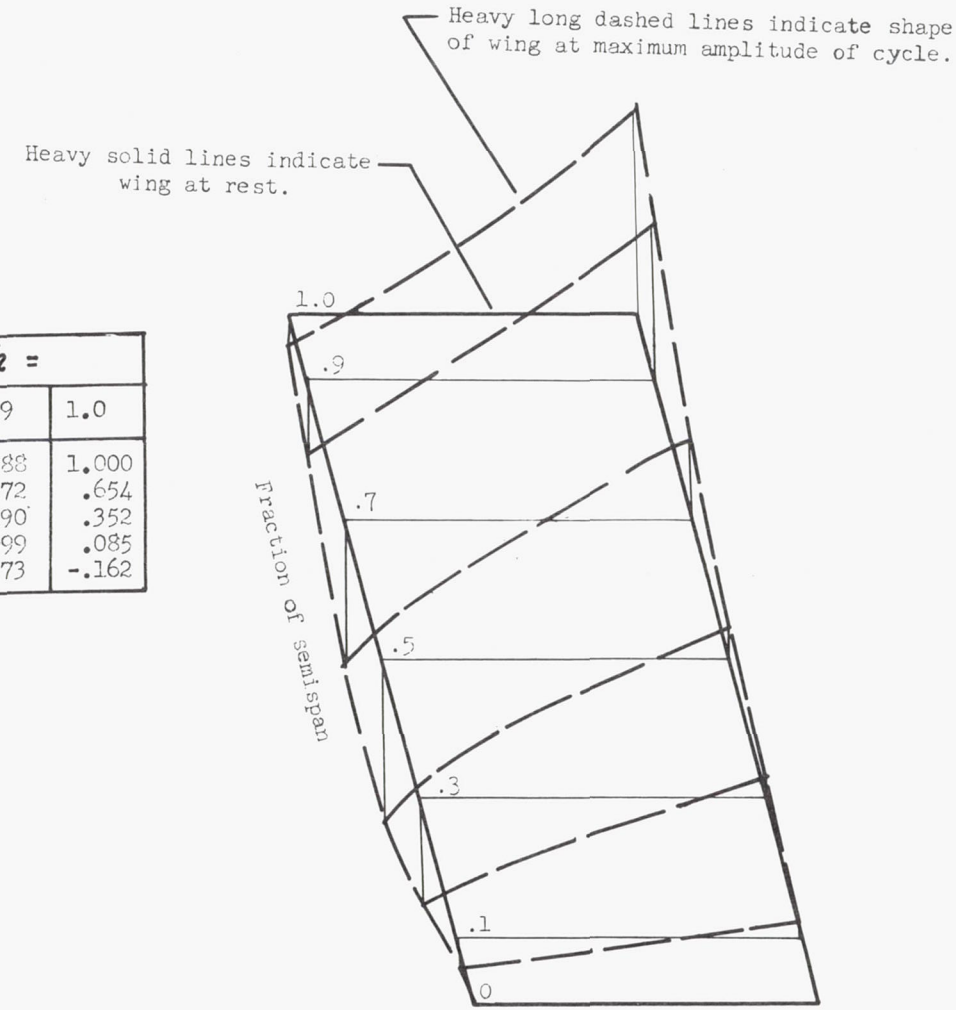

(c) Third natural vibration mode; f_3 = 238 cycles per second.

Figure 8.- Concluded.

Fraction of chord	Normalized deflection at y/l =					
	.1	.3	.5	.7	.9	1.0
0.00	.011	.052	.126	.233	.383	.472
.25	.015	.067	.148	.267	.420	.509
.50	.018	.080	.170	.296	.461	.625
.75	.025	.098	.195	.328	.518	.778
1.00	.030	.118	.226	.370	.604	1.000

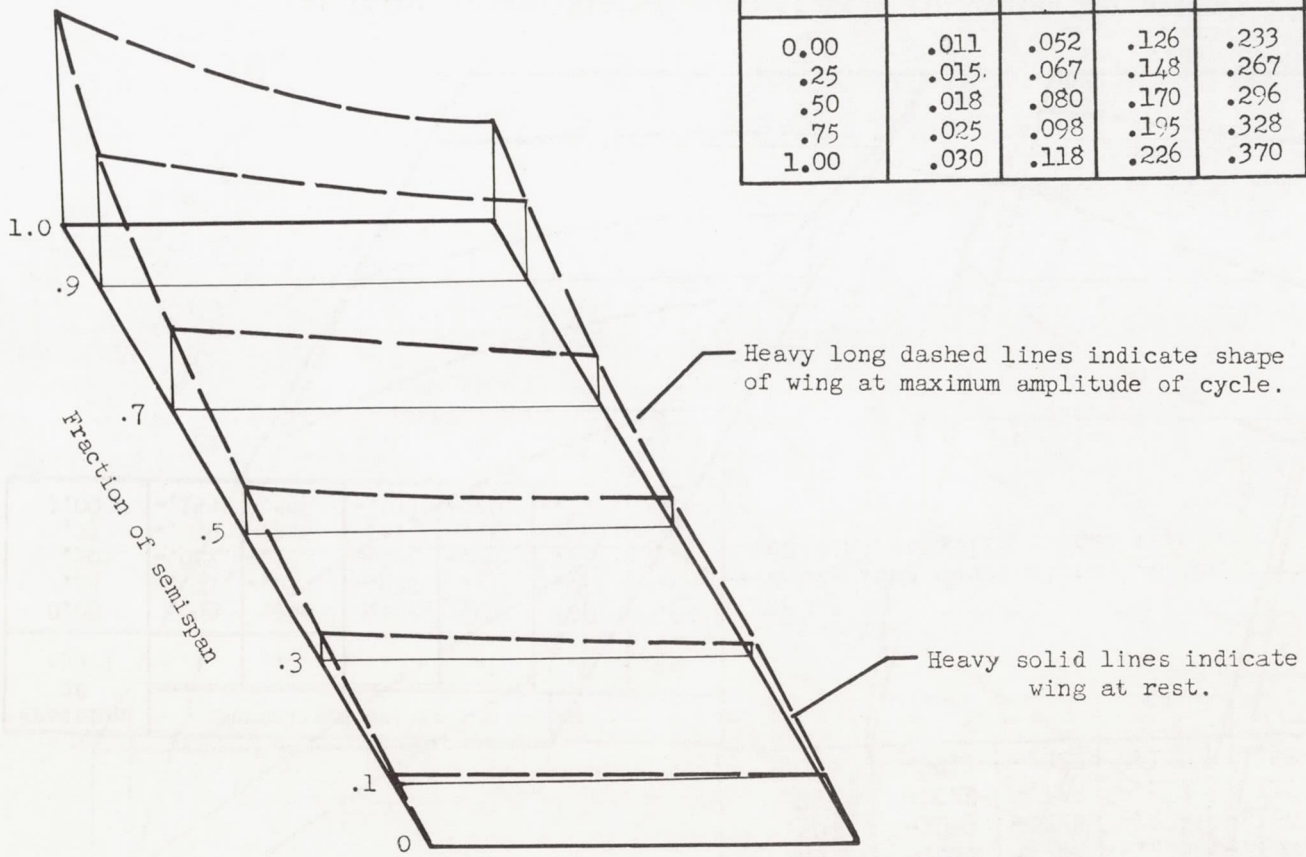

(a) First natural vibration mode; f_1 = 39 cycles per second.

Figure 9.- Natural vibration modes for magnesium flat-plate model. $\Lambda = 30^{\circ}$; $\lambda = 1.0$; $t/2b = 0.018$; $A = 4.15$.

Fraction of chord	Normalized deflection at y/l =					
	.1	.3	.5	.7	.9	1.0
0.00	-.025	-.264	-.494	-.563	-.500	-.361
.25	-.031	-.264	-.405	-.400	-.222	-.028
.50	-.033	-.228	-.295	-.160	.110	.300
.75	-.028	-.125	-.117	.147	.458	.630
1.00	-.011	-.022	.111	.458	.816	1.000

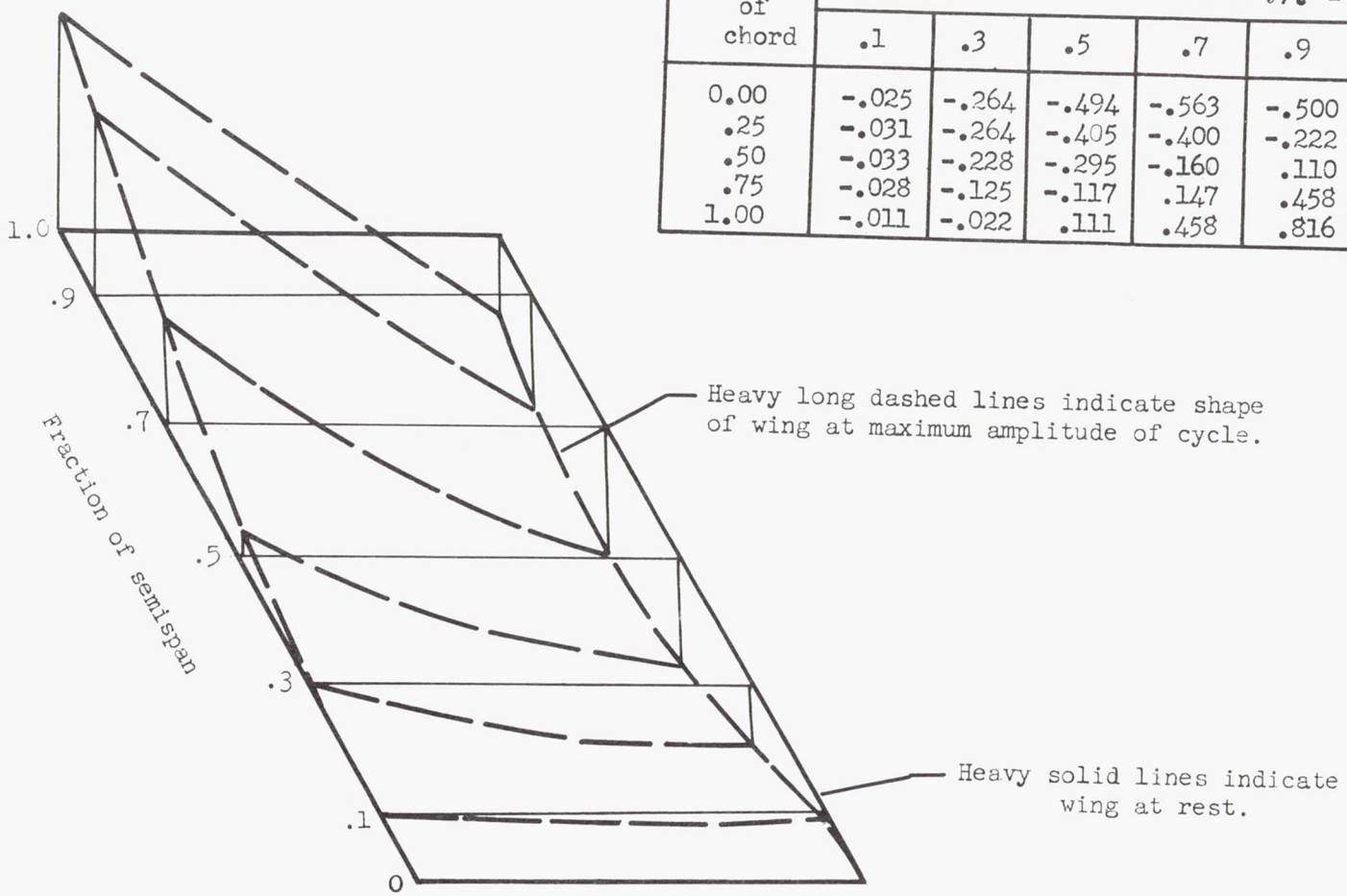

(b) Second natural vibration mode; f_2 = 212 cycles per second.

Figure 9.- Continued.

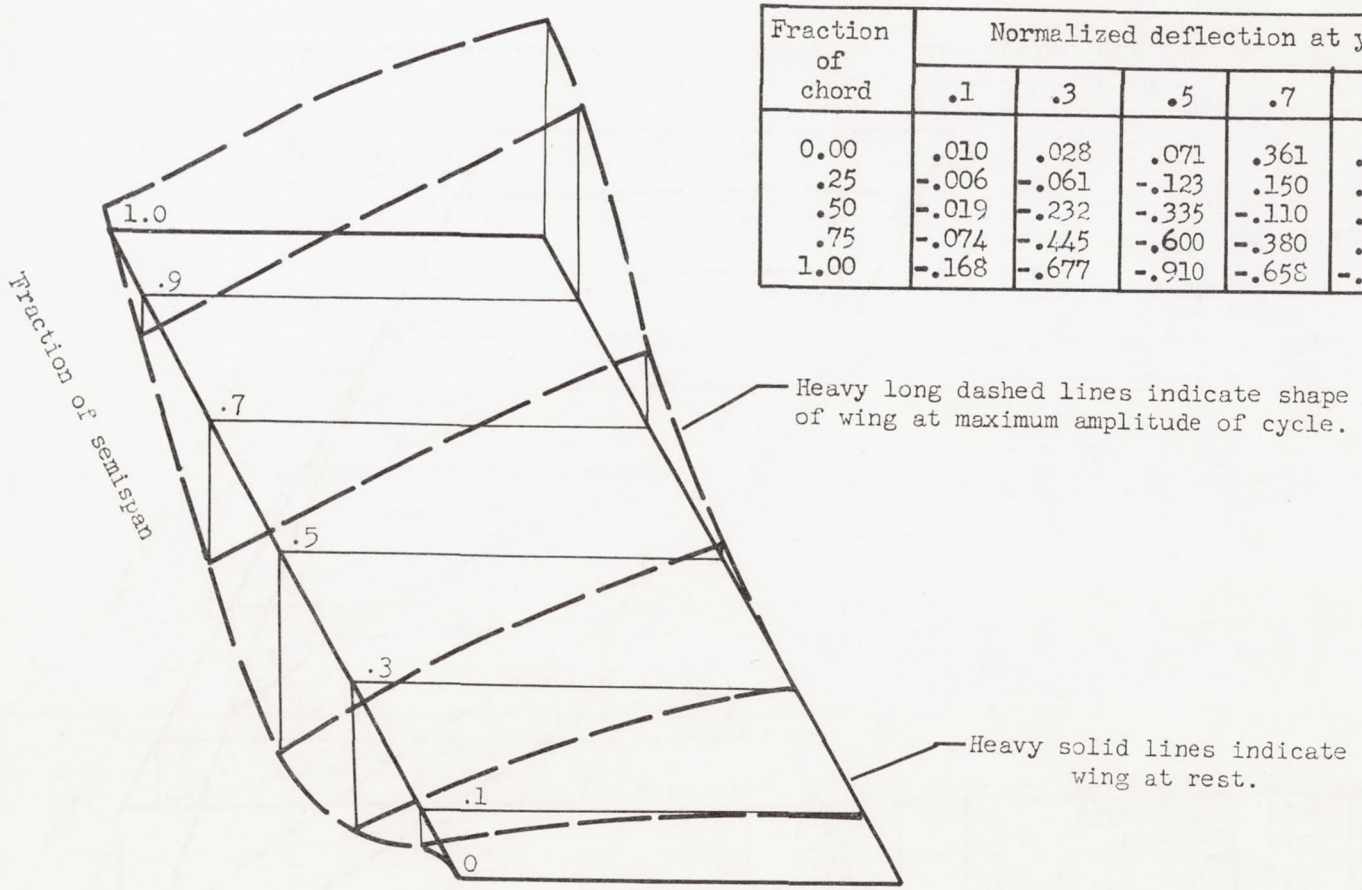

Fraction of chord	Normalized deflection at y/ℓ =					
	.1	.3	.5	.7	.9	1.0
0.00	.010	.028	.071	.361	.787	1.000
.25	-.006	-.061	-.123	.150	.600	.830
.50	-.019	-.232	-.335	-.110	.380	.613
.75	-.074	-.445	-.600	-.380	.070	.355
1.00	-.168	-.677	-.910	-.658	-.193	.097

(c) Third natural vibration mode; f_3 = 272 cycles per second.

Figure 9.- Concluded.

Fraction of chord	Normalized deflection at y/ℓ =					
	.1	.3	.5	.7	.9	1.0
0.00	.007	.054	.124	.210	.350	.467
.25	.017	.070	.155	.259	.418	.557
.50	.021	.091	.191	.313	.510	.673
.75	.028	.117	.238	.395	.640	.810
1.00	.039	.159	.307	.500	.812	1.000

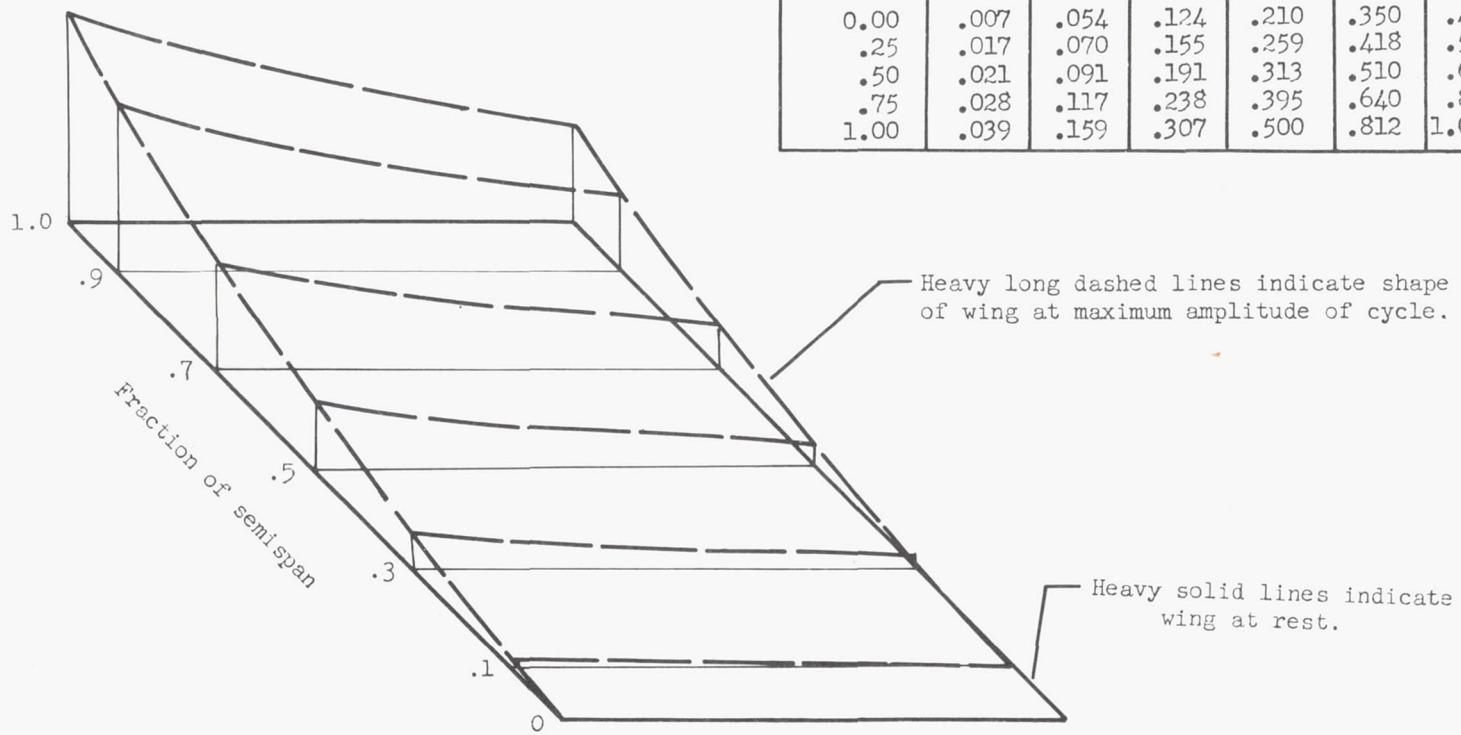

(a) First natural vibration mode; f_1 = 58 cycles per second.

Figure 10.- Natural vibration modes for magnesium flat-plate model. $\Lambda = 45^{\circ}$; $\lambda = 1.0$; $t/2b = 0.014$; $A = 2.76$.

Fraction of chord	Normalized deflection at y/ℓ =					
	.1	.3	.5	.7	.9	1.0
0.00	.007	.132	.578	.872	.904	.857
.25	.021	.286	.625	.718	.668	.607
.50	.046	.300	.471	.403	.014	-.143
.75	.050	.179	.057	-.282	-.678	-.786
1.00	-.036	-.196	-.518	-.793	-.947	-1.000

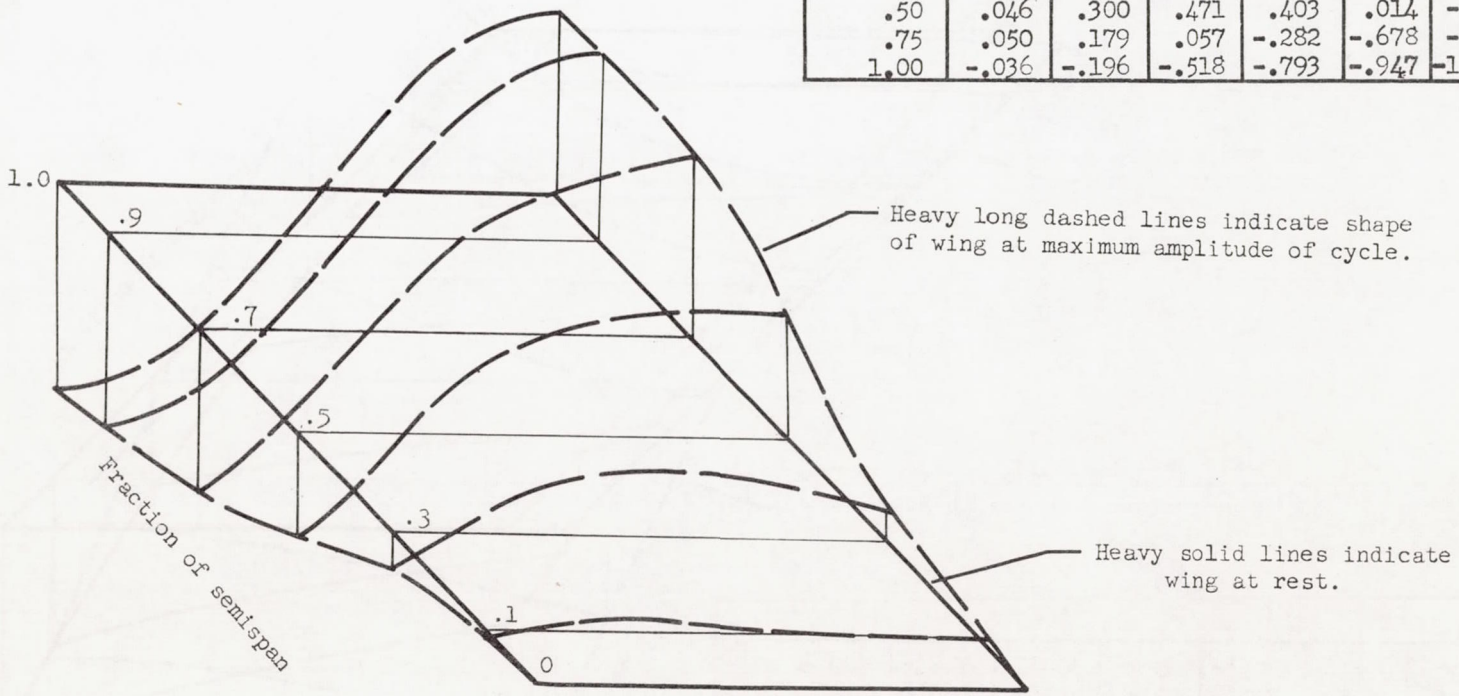

(b) Second natural vibration mode; f_2 = 184 cycles per second.

Figure 10.- Continued.

Fraction of chord	Normalized deflection at y/ℓ =					
	.1	.3	.5	.7	.9	1.0
0.00	.000	-.017	-.071	.063	.622	1.000
.25	-.004	-.059	-.185	-.029	.520	.840
.50	-.008	-.201	-.374	-.200	.416	.735
.75	-.050	-.470	-.676	-.412	.310	.681
1.00	-.214	-1.000	-1.000	-.504	.250	.651

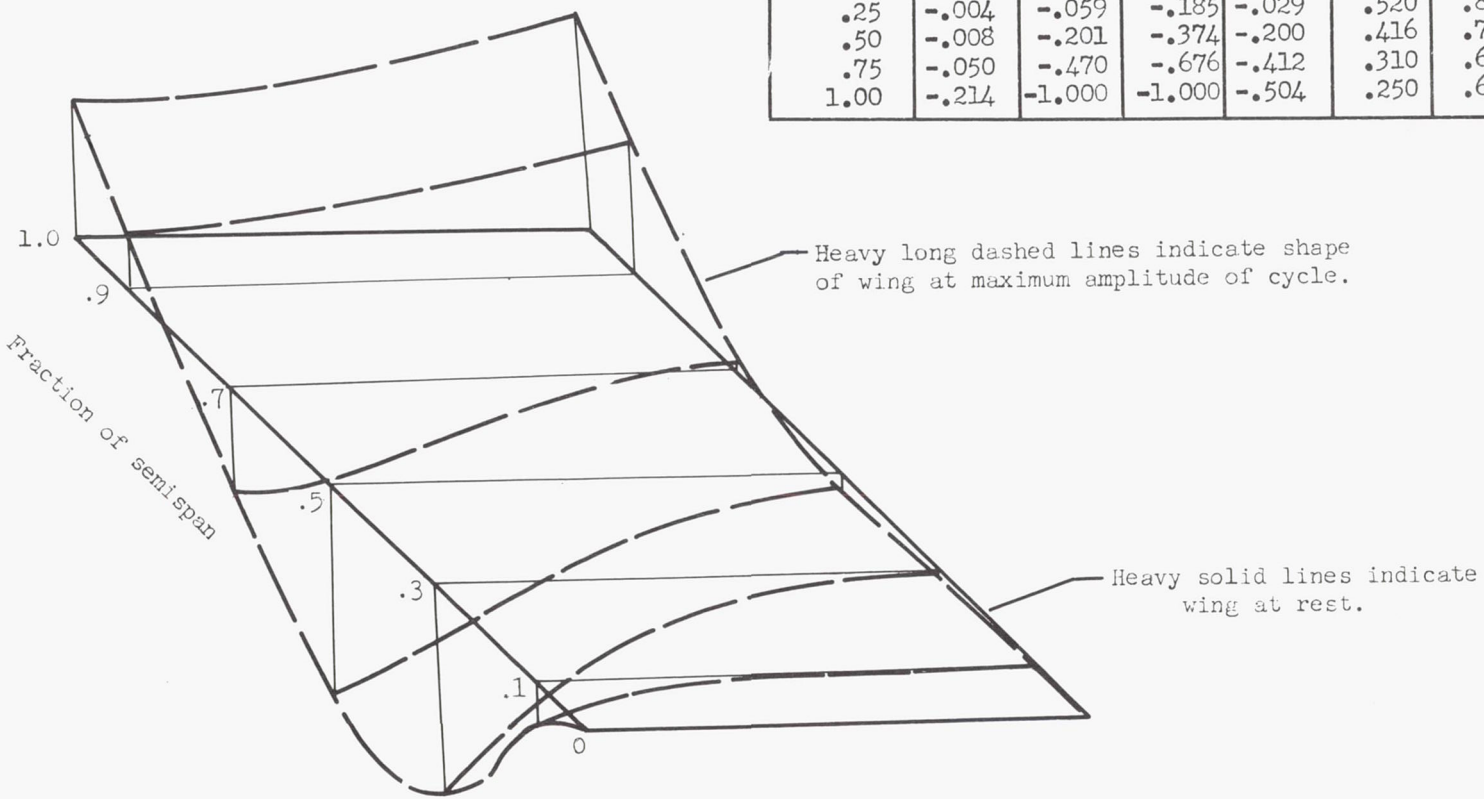

(c) Third natural vibration mode; f_3 = 263 cycles per second.

Figure 10.- Concluded.

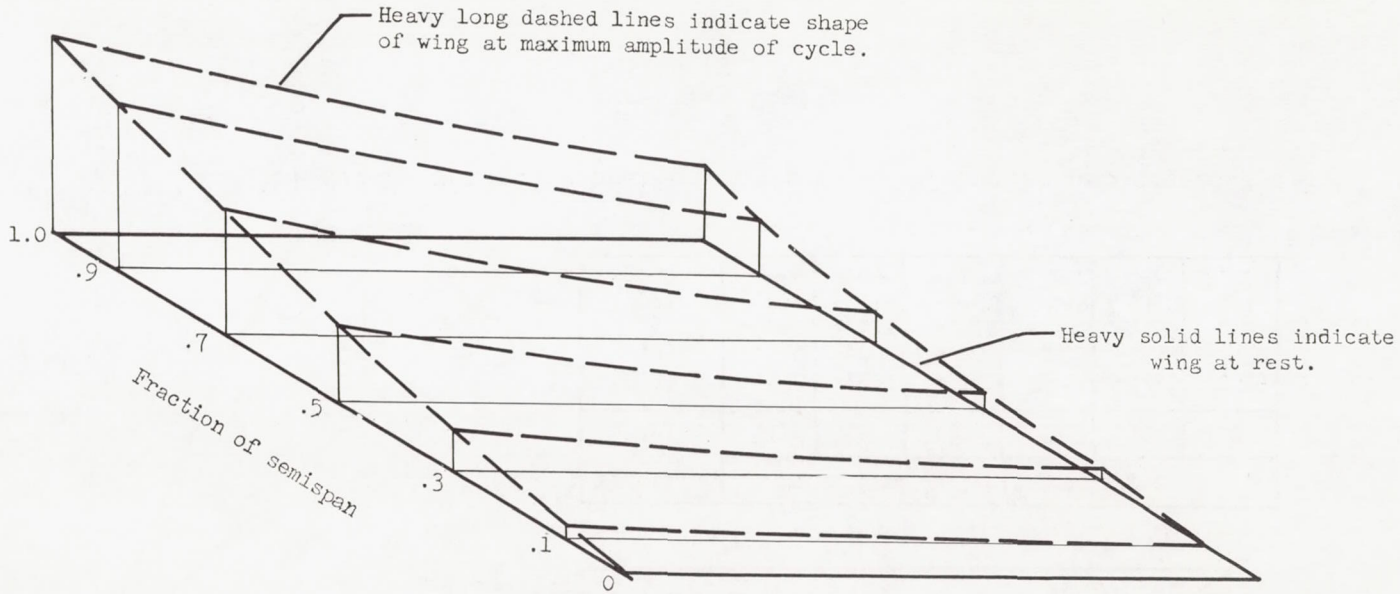

Fraction of chord	Normalized deflection at y/ℓ =					
	.1	.3	.5	.7	.9	1.0
0.00	.012	.040	.085	.164	.286	.380
.25	.015	.058	.116	.215	.376	.475
.50	.022	.091	.171	.315	.510	.620
.75	.040	.135	.272	.458	.665	.800
1.00	.062	.211	.400	.618	.830	1.000

(a) First natural vibration mode; f_1 = 47 cycles per second.

Figure 11.- Natural vibration modes for magnesium flat-plate model. $\Lambda = 60^{\circ}$; $\lambda = 1.0$; $t/2b = 0.010$; $A = 1.39$.

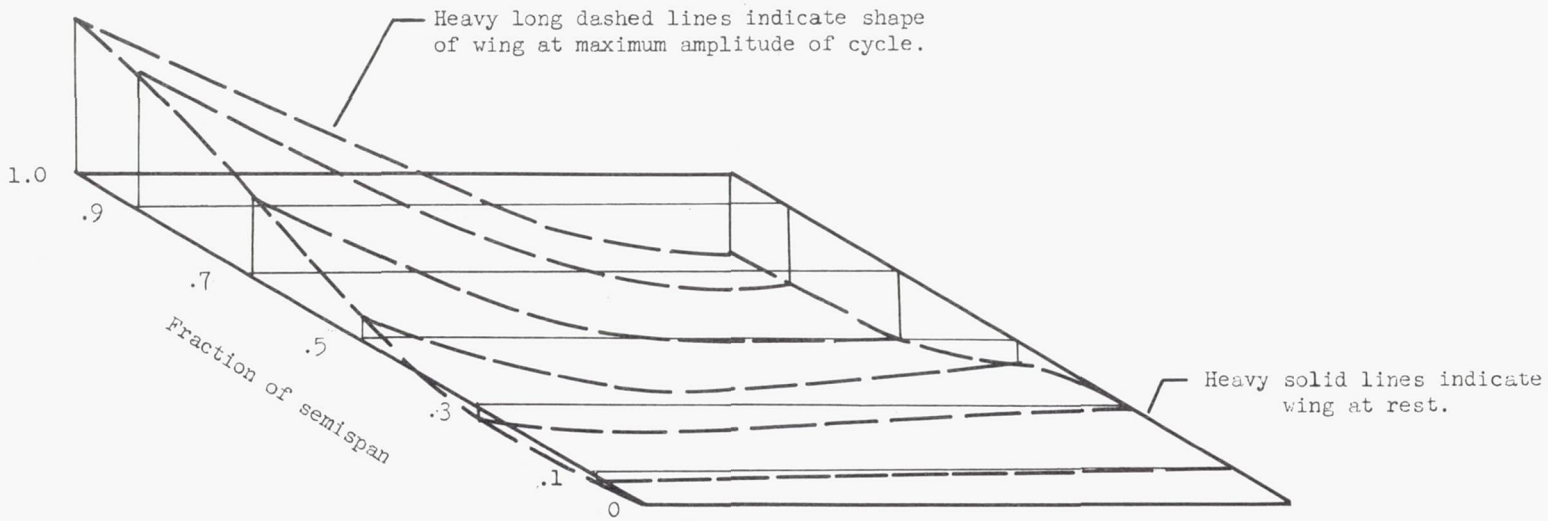

Fraction of chord	Normalized deflection at y/ℓ =					
	.1	.3	.5	.7	.9	1.0
0.00	-.008	-.039	-.156	-.383	-.495	-.515
.25	-.016	-.078	-.258	-.433	-.445	-.390
.50	-.022	-.133	-.312	-.328	-.156	.047
.75	-.034	-.159	-.180	.019	.350	.515
1.00	-.055	-.089	.109	.484	.867	1.000

(b) Second natural vibration mode; f_2 = 207 cycles per second.

Figure 11.- Continued.

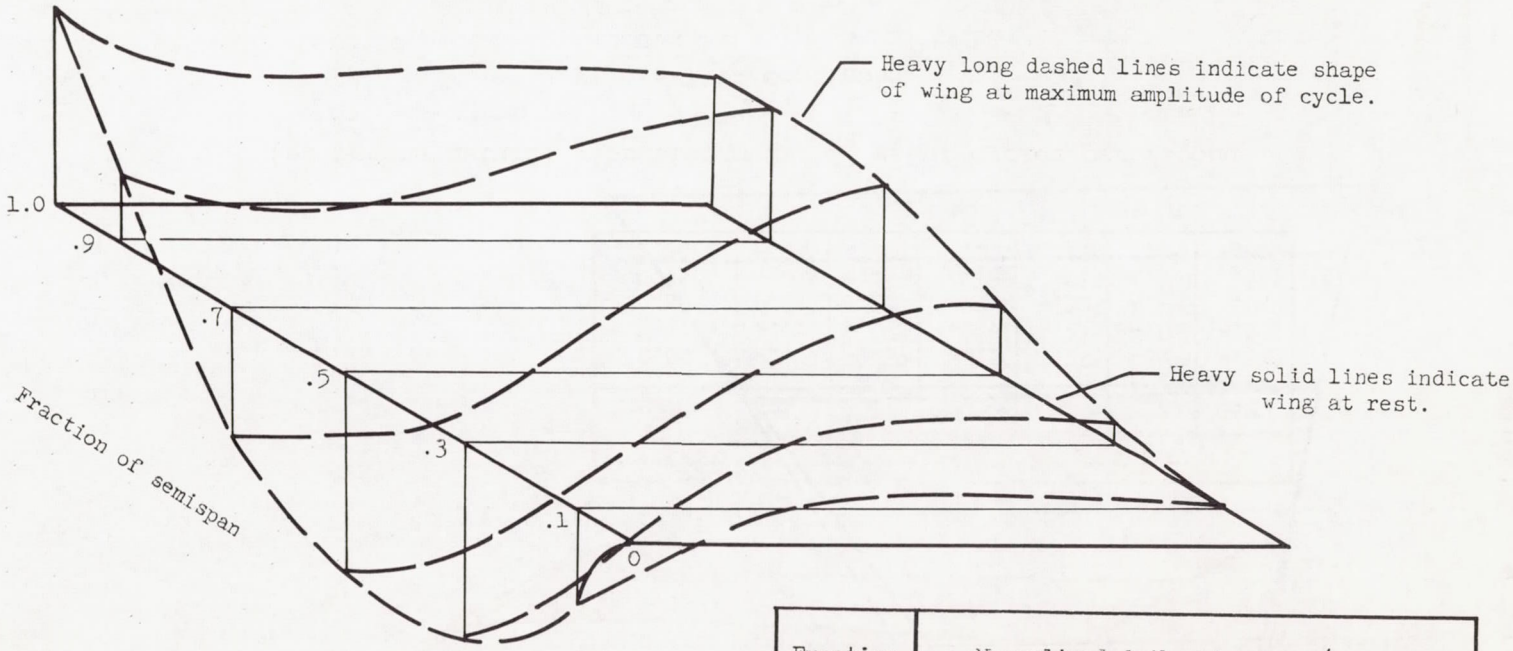

Fraction of chord	Normalized deflection at y/ℓ =					
	.1	.3	.5	.7	.9	1.0
0.00	-.024	-.111	-.347	-.606	-.667	-.650
.25	-.045	-.125	-.202	-.303	-.505	-.707
.50	-.071	.000	.238	.216	-.252	-.666
.75	.101	.545	.808	.657	-.162	-.656
1.00	.465	.980	1.000	.657	-.353	-1.000

(c) Third natural vibration mode; f_3 = 380 cycles per second.

Figure 11.- Concluded.

Fraction of chord	Normalized deflection at y/ℓ =					
	.1	.3	.5	.7	.9	1.0
0.00	.003	.061	.180	.360	.686	.978
.25	.004	.065	.183	.368	.701	1.000
.50	.004	.065	.172	.356	.696	.985
.75	.002	.057	.164	.341	.676	.950
1.00	.001	.039	.151	.324	.640	.882

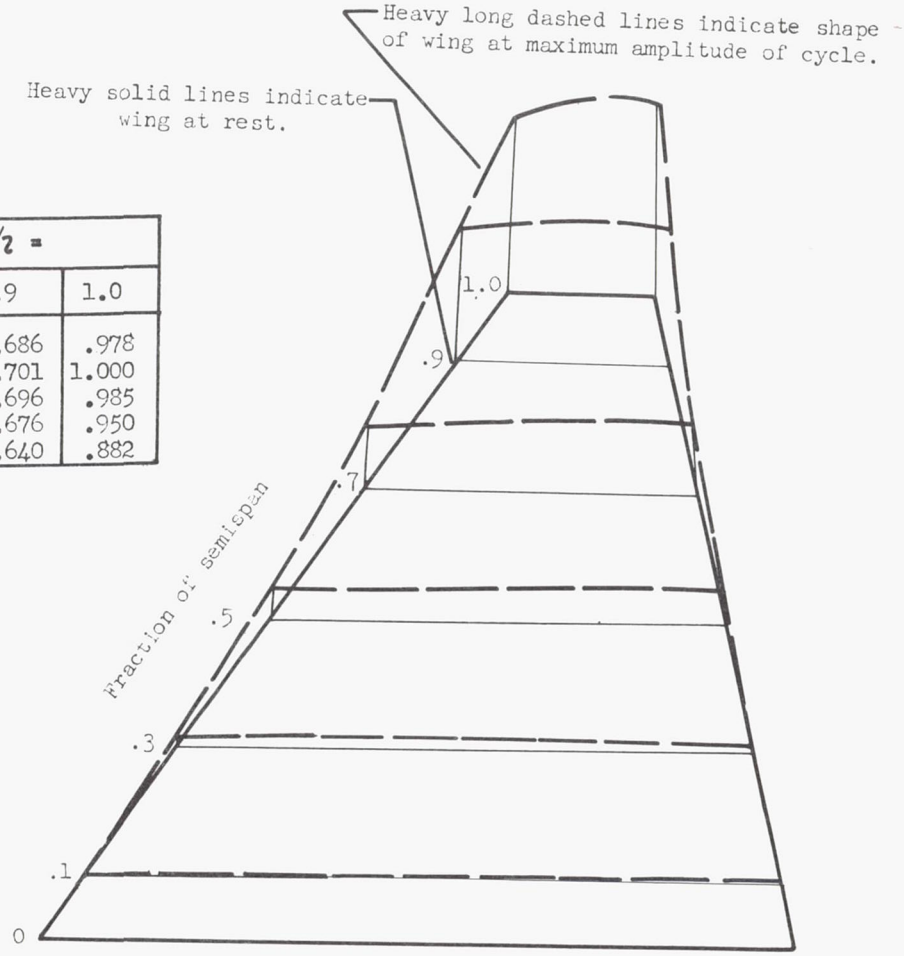

(a) First natural vibration mode; f_1 = 125 cycles per second.

Figure 12.- Natural vibration modes for magnesium model with NACA 65A section. $\Lambda = 0^{\circ}$; $\lambda = 0.20$; $t/2b = 0.02$; $A = 4.0$.

Fraction of chord	Normalized deflection at y/l =					
	.1	.3	.5	.7	.9	1.0
0.00	-.000	-.082	-.246	-.108	.540	1.000
.25	-.013	-.108	-.246	-.119	.494	.924
.50	-.016	-.109	-.254	-.151	.457	.886
.75	-.012	-.093	-.264	-.200	.436	.870
1.00	-.002	-.065	-.277	-.259	.424	.865

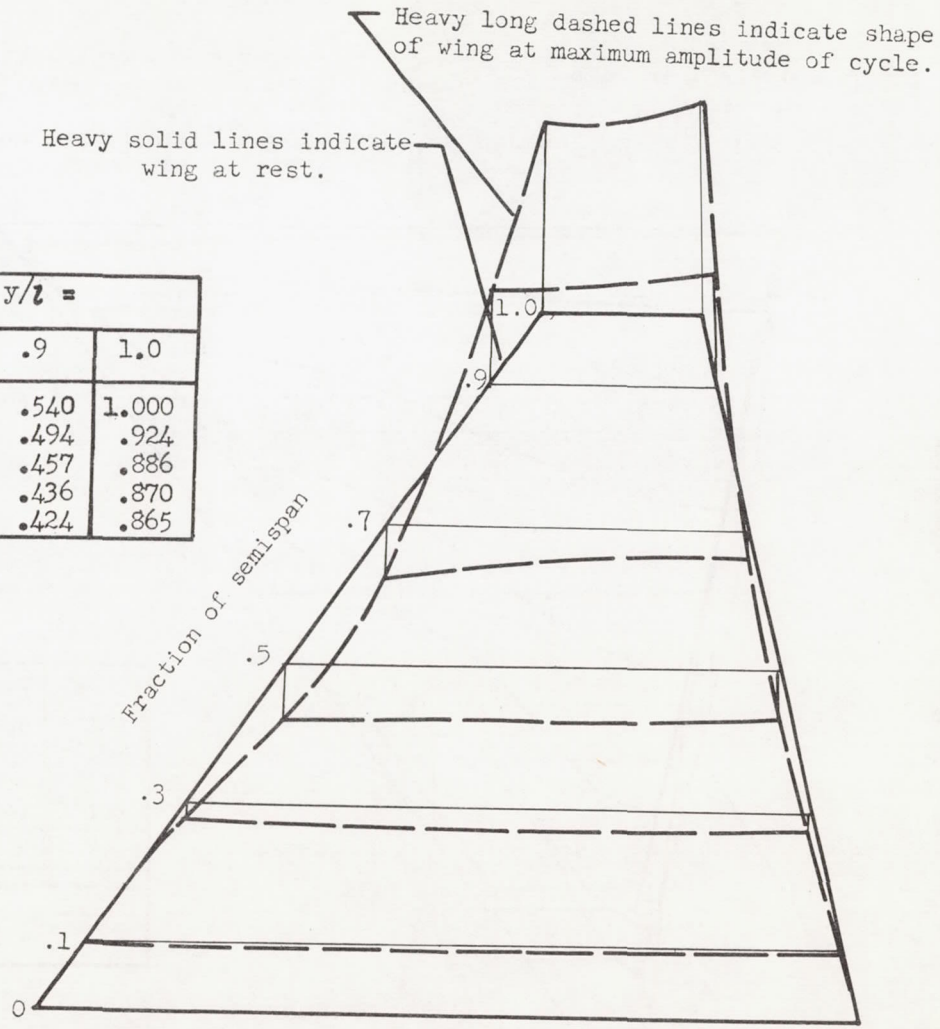

(b) Second natural vibration mode; f_2 = 370 cycles per second.

Figure 12.- Continued.

Fraction of chord	Normalized deflection at y/ℓ =					
	.1	.3	.5	.7	.9	1.0
0.00	.074	.586	.774	.767	.621	.472
.25	.050	.346	.568	.614	.363	.145
.50	-.021	-.076	-.084	-.114	-.227	-.363
.75	-.059	-.451	-.544	-.558	-.636	-.799
1.00	-.074	-.521	-.675	-.683	-.817	-1.000

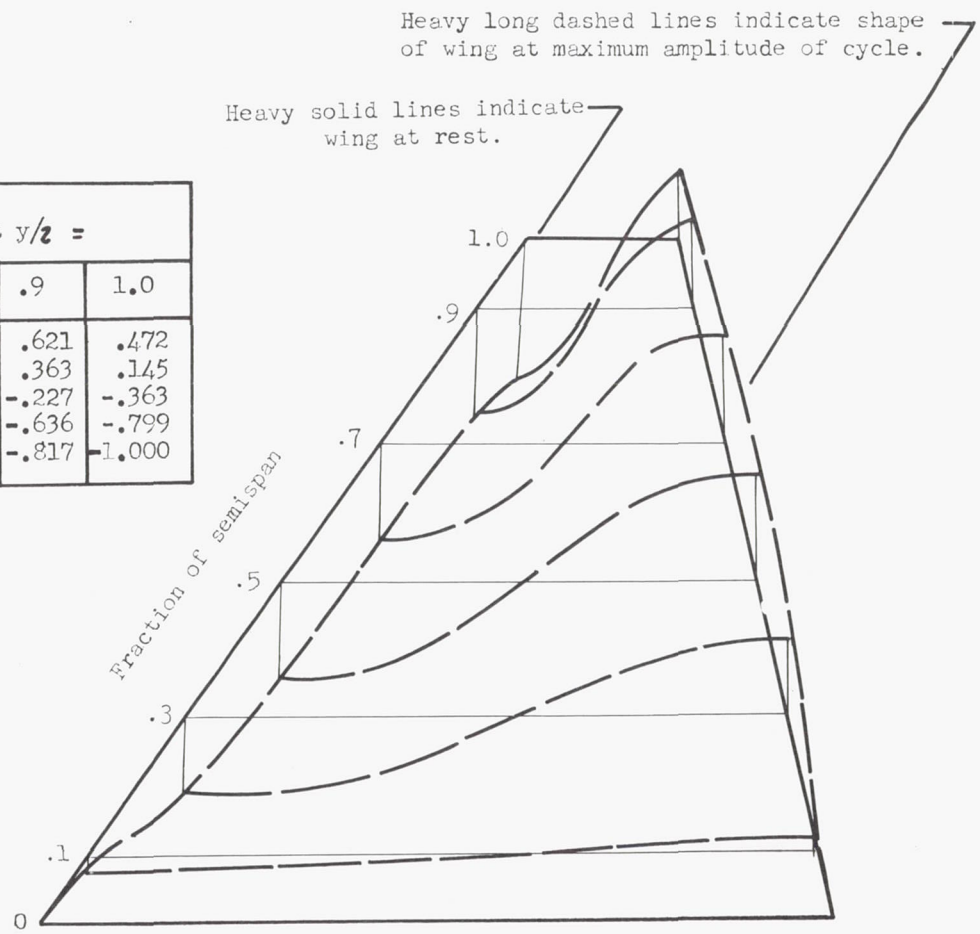

(c) Third natural vibration mode; f_3 = 510 cycles per second.

Figure 12.- Concluded.

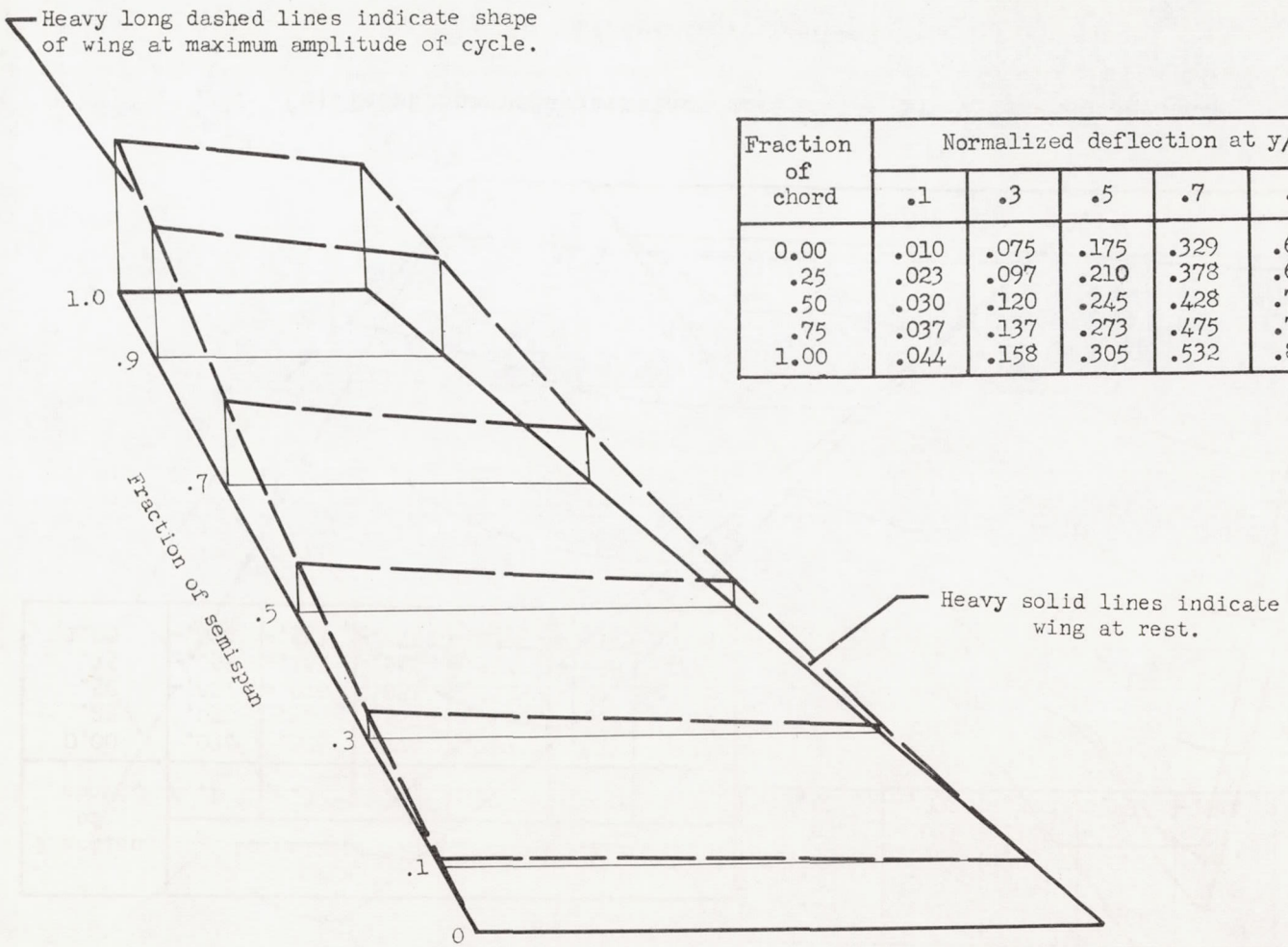

Fraction of chord	Normalized deflection at y/ℓ =					
	.1	.3	.5	.7	.9	1.0
0.00	.010	.075	.175	.329	.606	.788
.25	.023	.097	.210	.378	.674	.844
.50	.030	.120	.245	.428	.729	.896
.75	.037	.137	.273	.475	.771	.946
1.00	.044	.158	.305	.532	.830	1.000

(a) First natural vibration mode; f_1 = 95 cycles per second.

Figure 13.- Natural vibration modes for wood model with NACA 65A section. $\Lambda = 45^{\circ}$; $\lambda = 0.4$; $t/2b = 0.04$; $A = 4.0$.

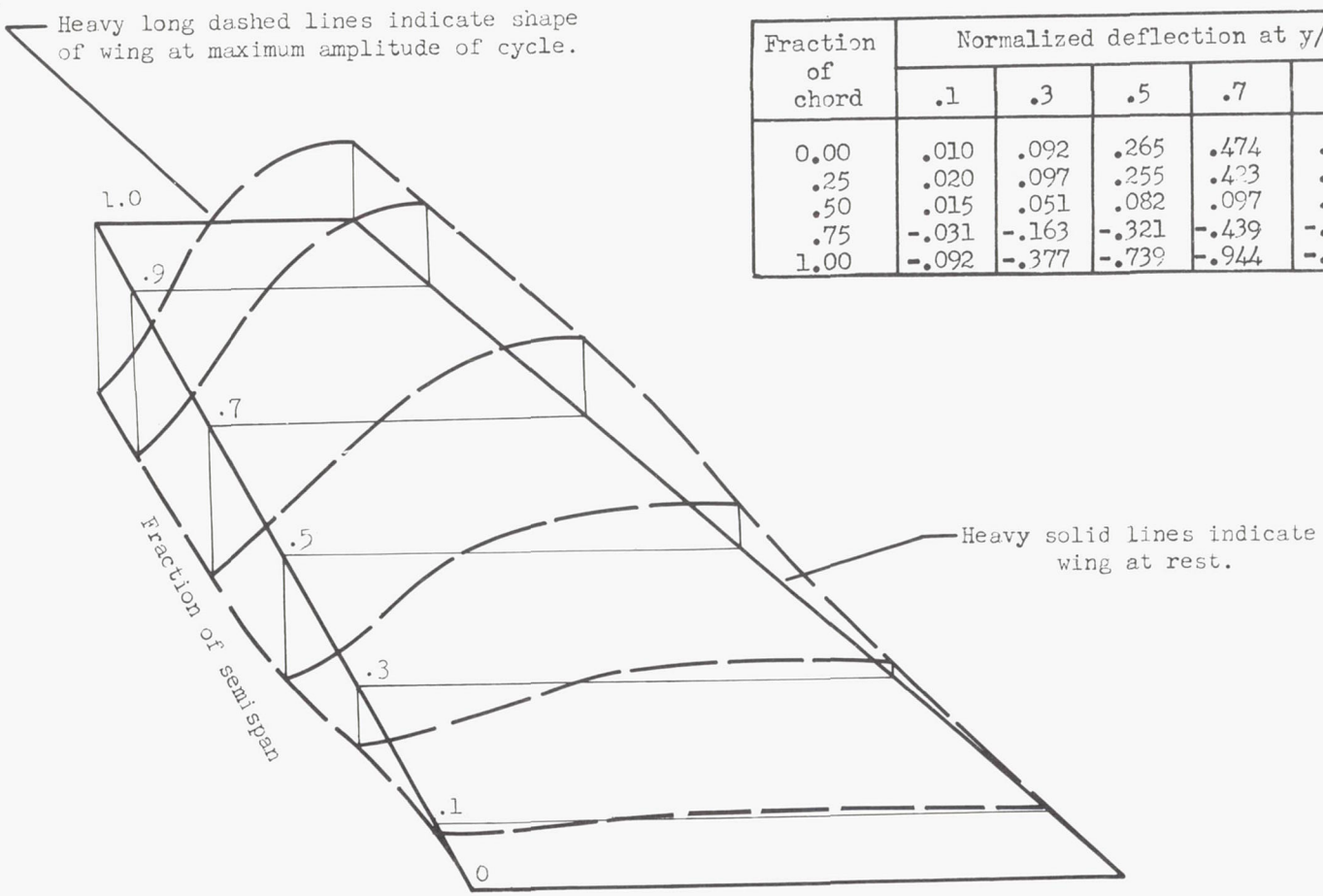

Fraction of chord	Normalized deflection at y/l =					
	.1	.3	.5	.7	.9	1.0
0.00	.010	.092	.265	.474	.479	.480
.25	.020	.097	.255	.423	.408	.393
.50	.015	.051	.082	.097	.102	.089
.75	-.031	-.163	-.321	-.439	-.500	-.510
1.00	-.092	-.377	-.739	-.944	-.995	-1.000

(b) Second natural vibration mode; f_2 = 326 cycles per second.

Figure 13.- Continued.

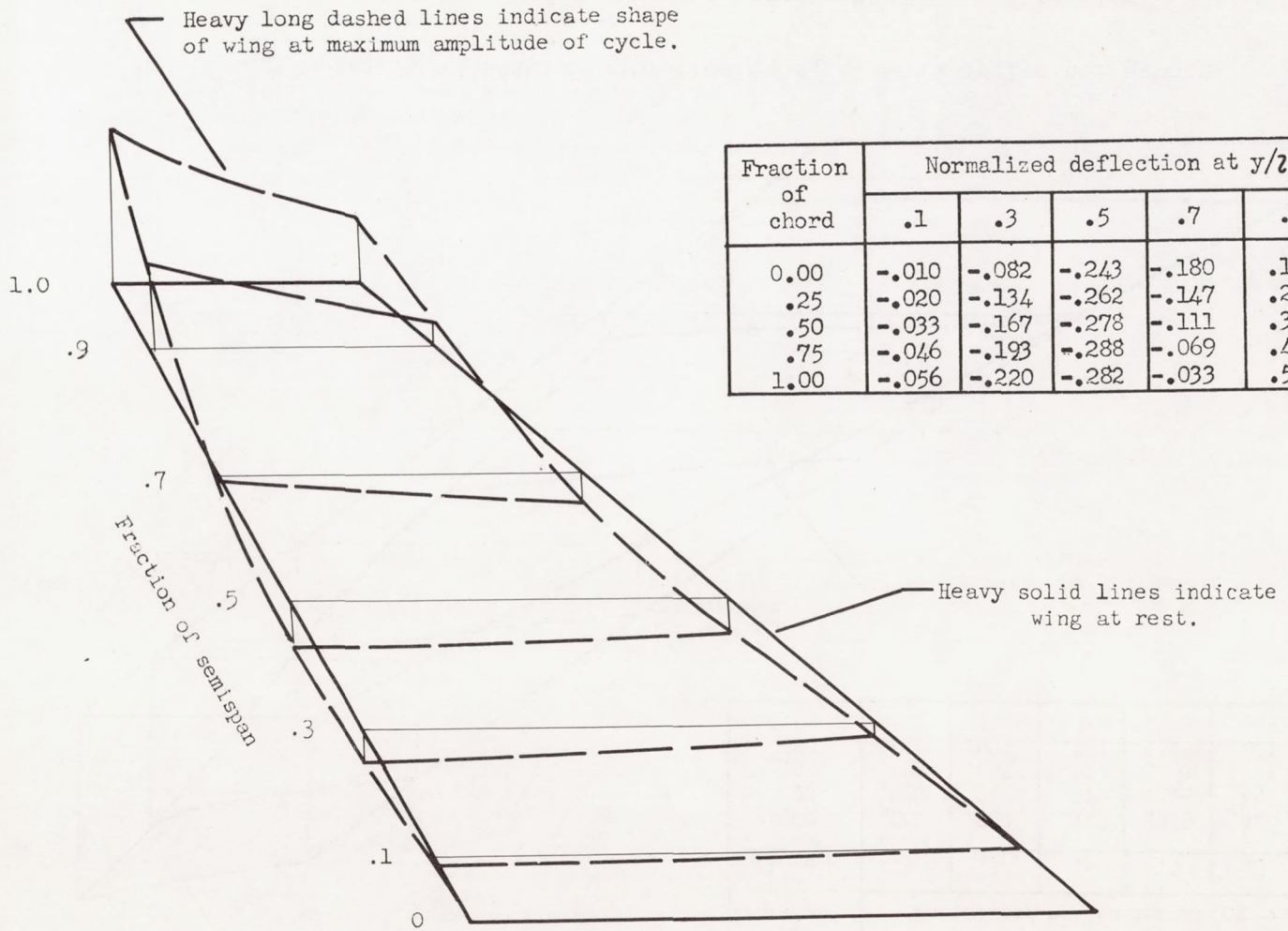

Fraction of chord	Normalized deflection at y/l =					
	.1	.3	.5	.7	.9	1.0
0.00	-.010	-.082	-.243	-.180	.147	.416
.25	-.020	-.134	-.262	-.147	.239	.518
.50	-.033	-.167	-.278	-.111	.338	.639
.75	-.046	-.193	-.288	-.069	.436	.787
1.00	-.056	-.220	-.282	-.033	.541	1.000

(c) Third natural vibration mode; f_3 = 390 cycles per second.

Figure 13.- Concluded.

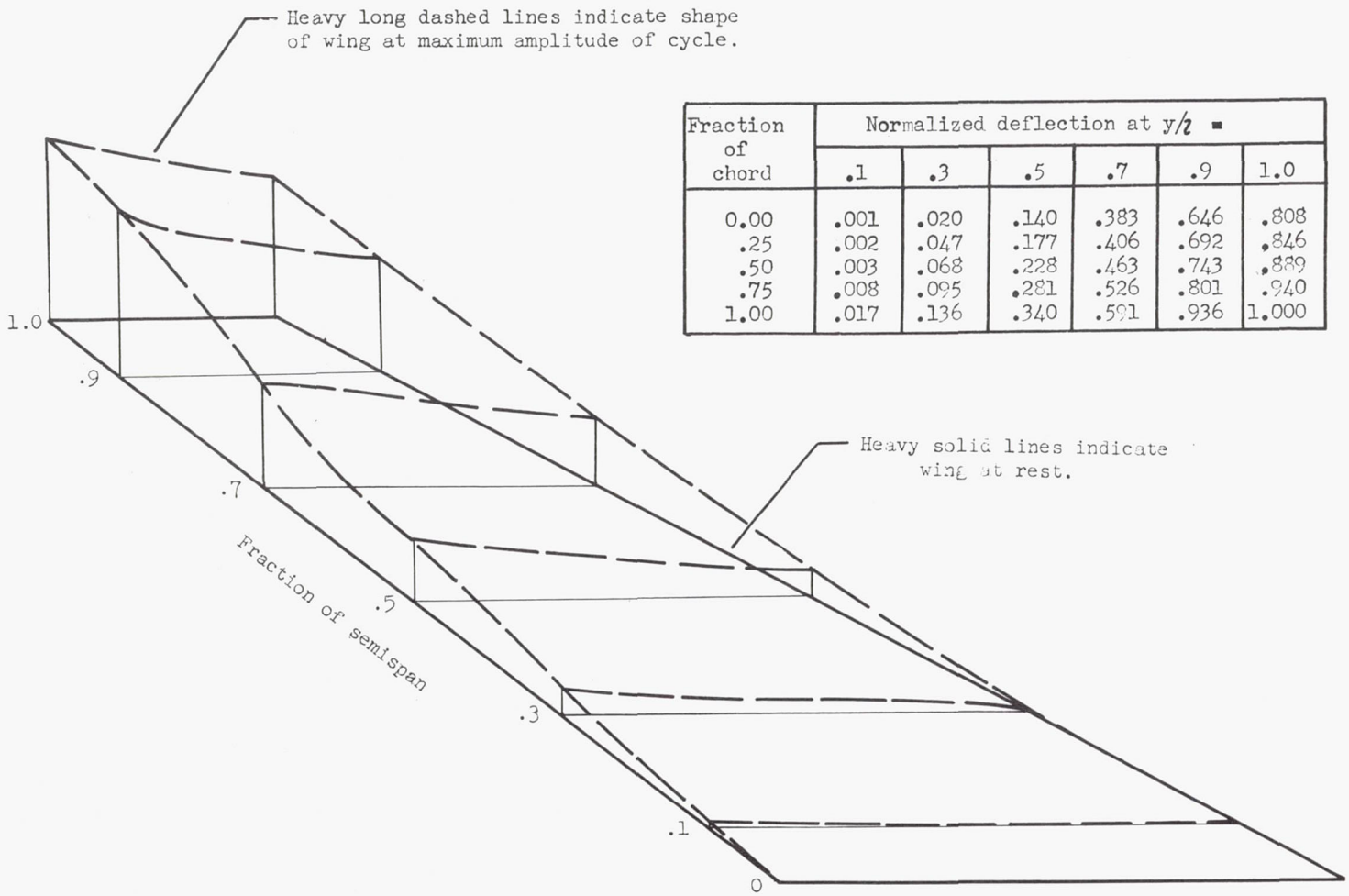

Fraction of chord	Normalized deflection at y/ℓ =					
	.1	.3	.5	.7	.9	1.0
0.00	.001	.020	.140	.383	.646	.808
.25	.002	.047	.177	.406	.692	.846
.50	.003	.068	.228	.463	.743	.889
.75	.008	.095	.281	.526	.801	.940
1.00	.017	.136	.340	.591	.936	1.000

(a) First natural vibration mode; f_1 = 43 cycles per second.

Figure 14.- Natural vibration modes for wood model with NACA 65A section. $\Lambda = 60^{\circ}$; $\lambda = 0.4$; $t/2b = 0.04$; $A = 4.0$.

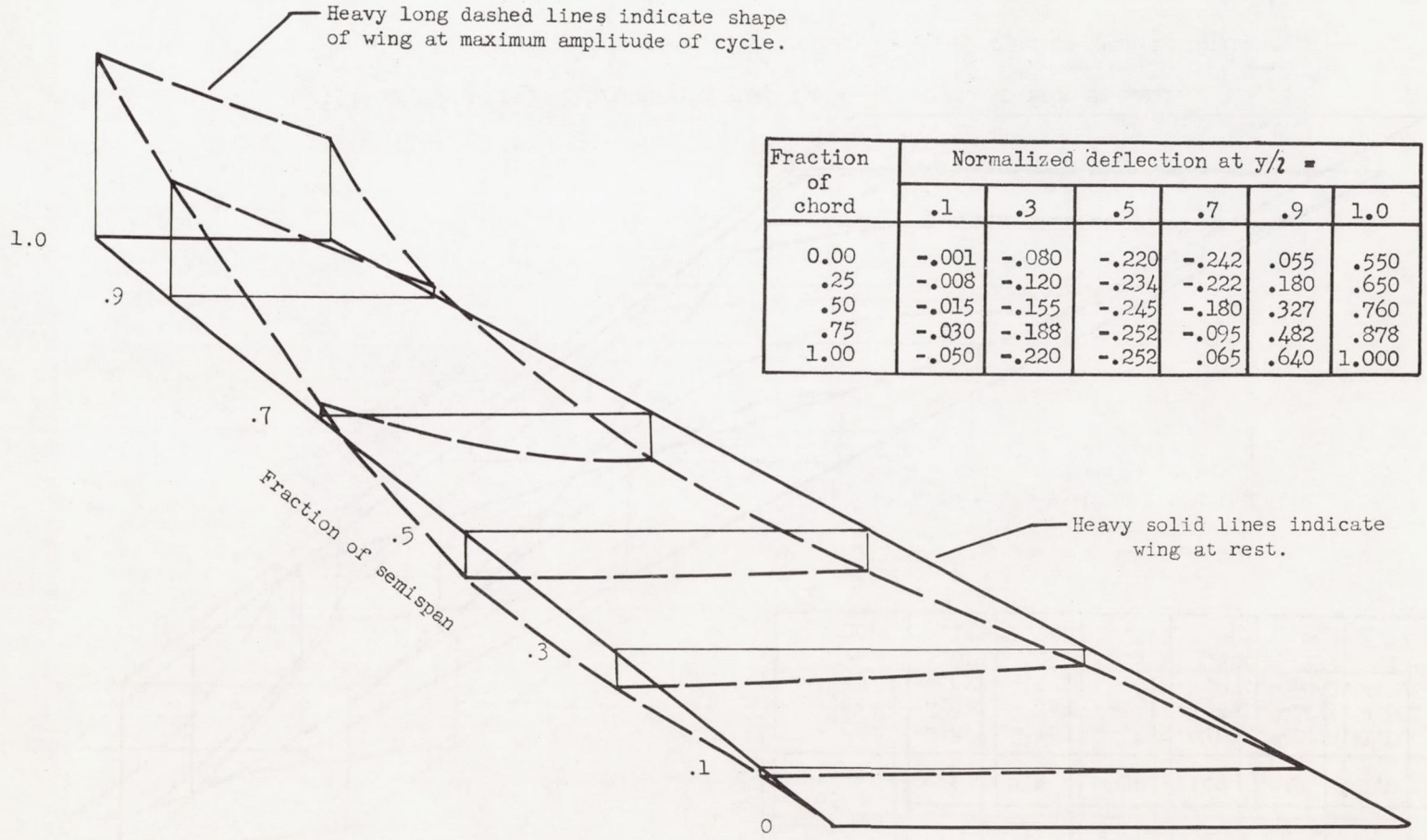

Fraction of chord	Normalized deflection at y/l =					
	.1	.3	.5	.7	.9	1.0
0.00	-.001	-.080	-.220	-.242	.055	.550
.25	-.008	-.120	-.234	-.222	.180	.650
.50	-.015	-.155	-.245	-.180	.327	.760
.75	-.030	-.188	-.252	-.095	.482	.878
1.00	-.050	-.220	-.252	.065	.640	1.000

(b) Second natural vibration mode; f_2 = 171 cycles per second.

Figure 14.- Continued.

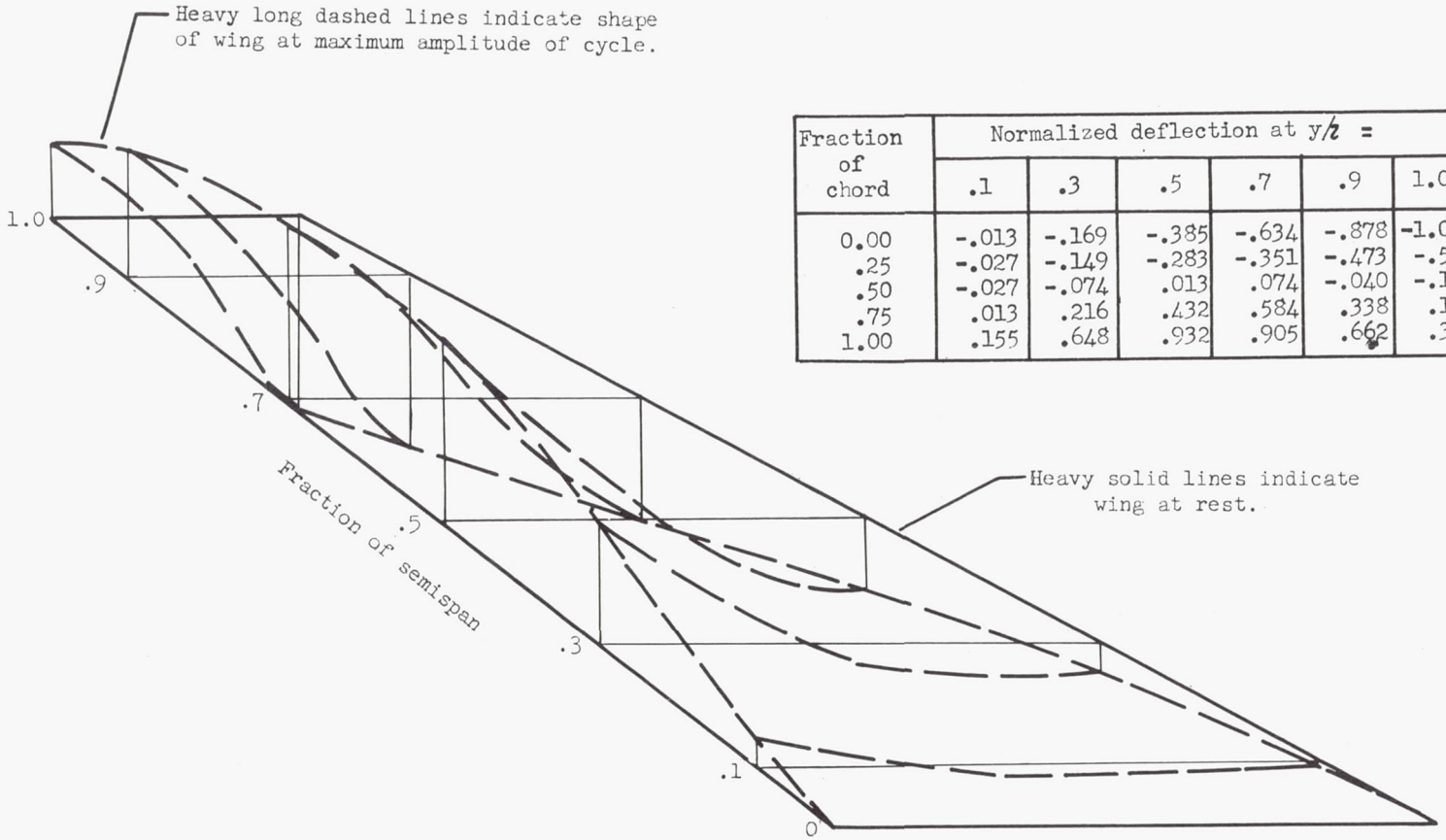

Fraction of chord	Normalized deflection at y/h =					
	.1	.3	.5	.7	.9	1.0
0.00	-.013	-.169	-.385	-.634	-.878	-1.000
.25	-.027	-.149	-.283	-.351	-.473	-.581
.50	-.027	-.074	.013	.074	-.040	-.176
.75	.013	.216	.432	.584	.338	.135
1.00	.155	.648	.932	.905	.662	.371

(c) Third natural vibration mode; f_3 = 328 cycles per second.

Figure 14.- Concluded.

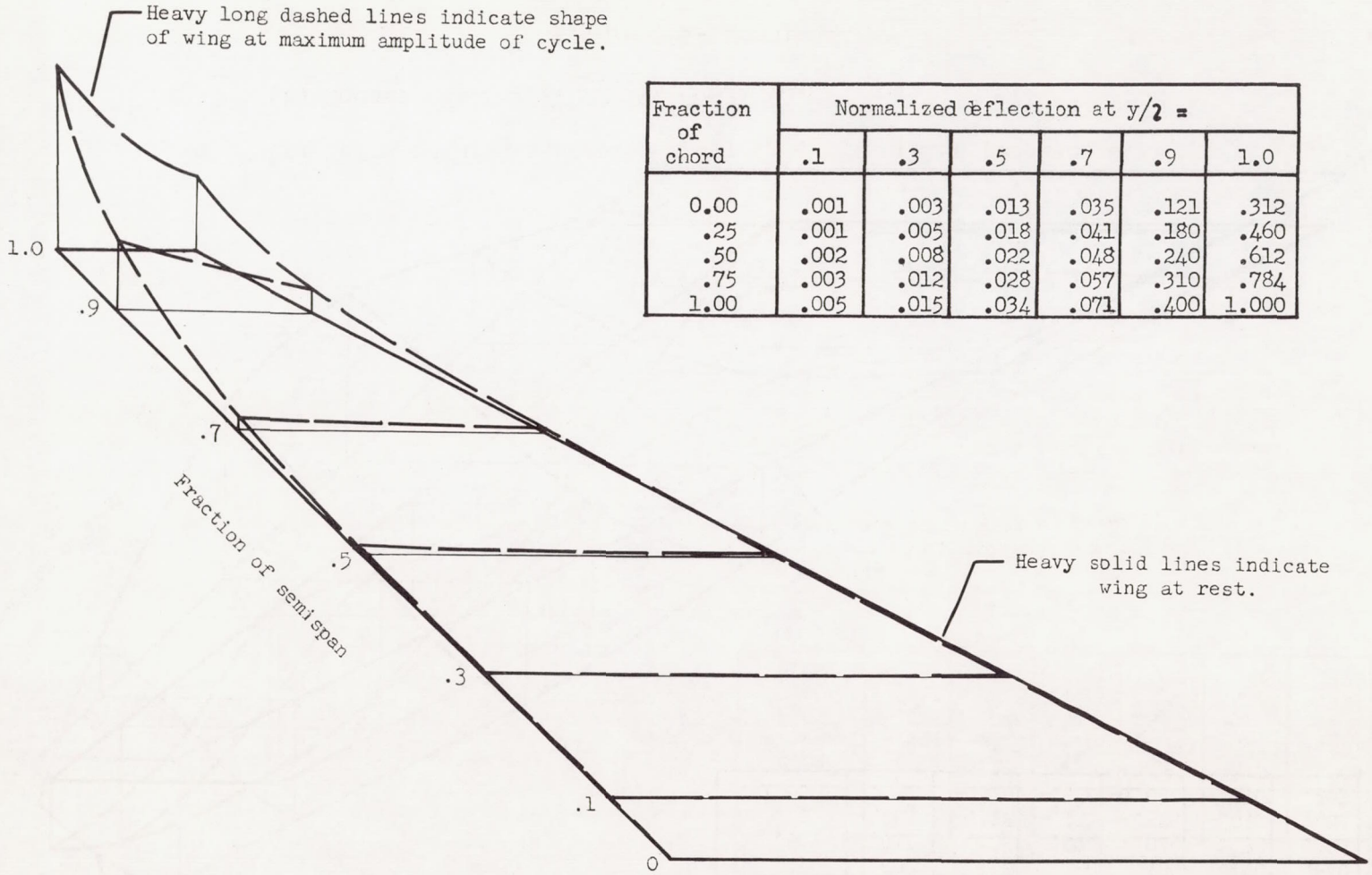

Fraction of chord	Normalized deflection at y/ℓ =					
	.1	.3	.5	.7	.9	1.0
0.00	.001	.003	.013	.035	.121	.312
.25	.001	.005	.018	.041	.180	.460
.50	.002	.008	.022	.048	.240	.612
.75	.003	.012	.028	.057	.310	.784
1.00	.005	.015	.034	.071	.400	1.000

(a) First natural vibration mode; f_1 = 74 cycles per second.

Figure 15.- Natural vibration modes for wood model with NACA 65A section. $\Lambda = 60^{\circ}$; $\lambda = 0.20$; $t/2b = 0.04$; $A = 4.0$.

Fraction of chord	Normalized deflection at y/l =					
	.1	.3	.5	.7	.9	1.0
0.00	.002	.120	.474	.650	.680	.680
.25	.007	.158	.390	.406	.450	.640
.50	.011	.128	.074	-.049	.178	.526
.75	-.004	-.128	-.411	-.583	-.090	.404
1.00	-.084	-.520	-.926	-1.000	-.316	.263

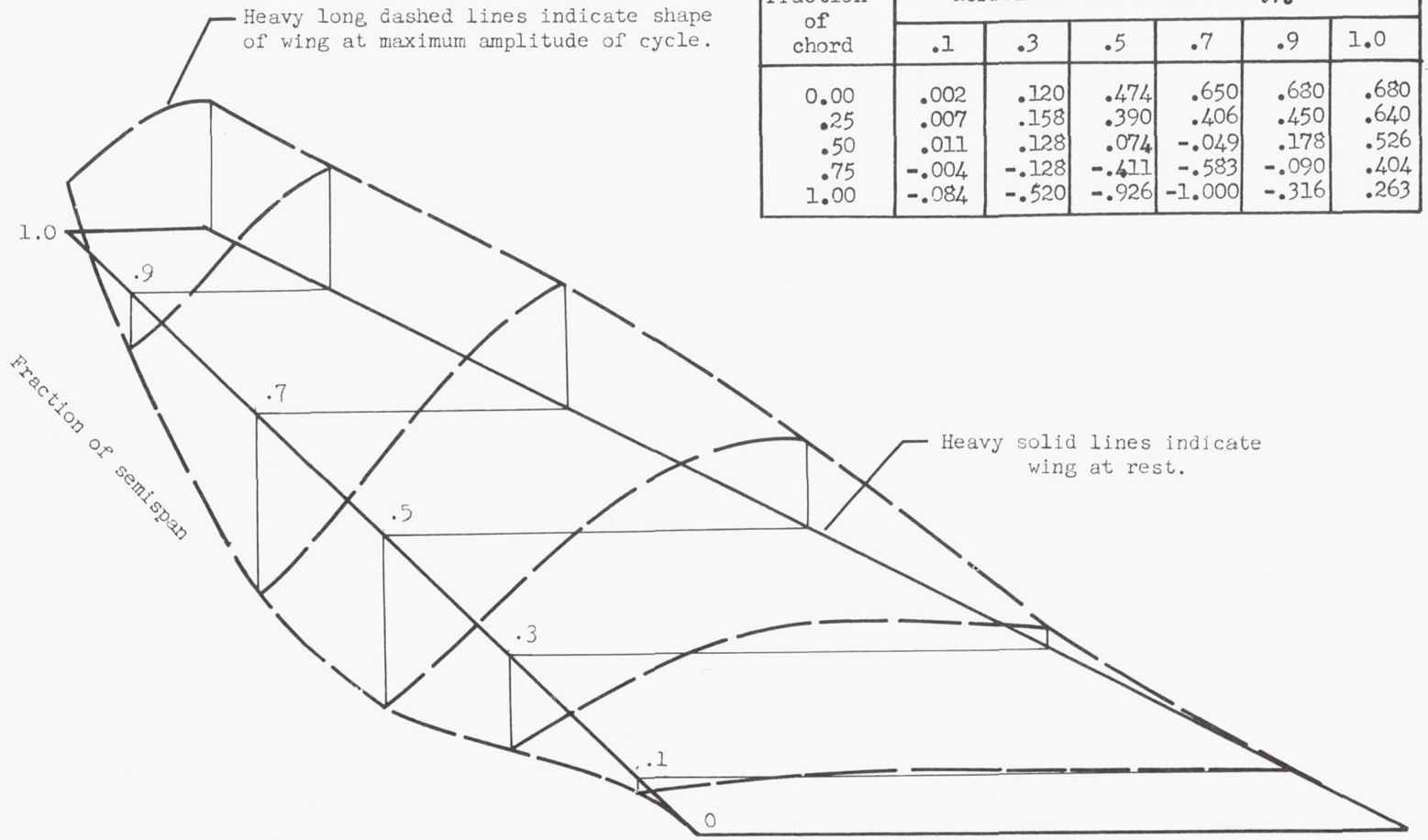

(b) Second natural vibration mode; f_2 = 208 cycles per second.

Figure 15.- Continued.

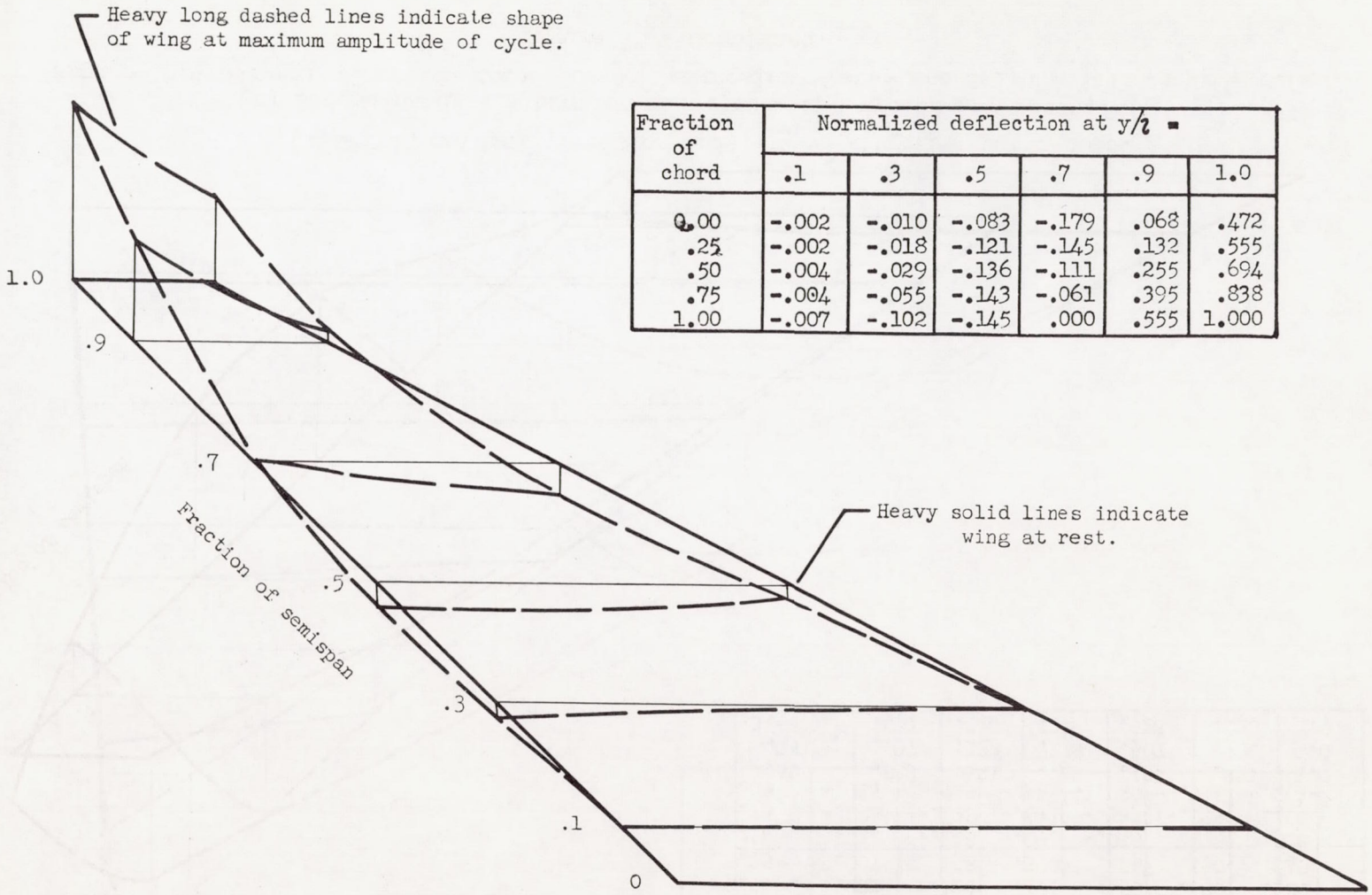

Fraction of chord	Normalized deflection at y/l =					
	.1	.3	.5	.7	.9	1.0
0.00	-.002	-.010	-.083	-.179	.068	.472
.25	-.002	-.018	-.121	-.145	.132	.555
.50	-.004	-.029	-.136	-.111	.255	.694
.75	-.004	-.055	-.143	-.061	.395	.838
1.00	-.007	-.102	-.145	.000	.555	1.000

(c) Third natural vibration mode; f_3 = 415 cycles per second.

Figure 15.- Concluded.

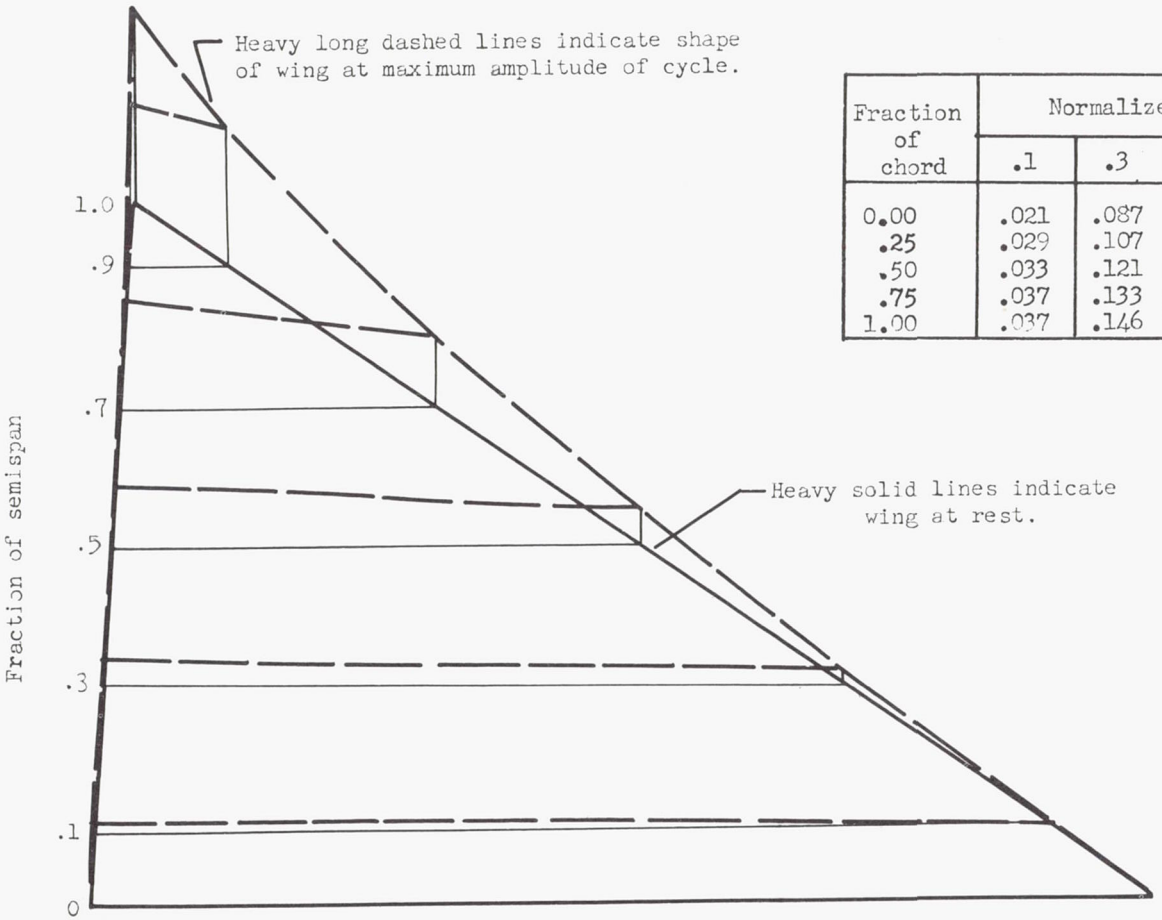

Fraction of chord	Normalized deflection at y/ℓ =					
	.1	.3	.5	.7	.9	1.0
0.00	.021	.087	.186	.357	.702	1.0
.25	.029	.107	.214	.400	.742	1.0
.50	.033	.121	.247	.453	.771	1.0
.75	.037	.133	.278	.507	.796	1.0
1.00	.037	.146	.297	.528	.820	1.0

(a) First natural vibration mode; f_1 = 50 cycles per second.

Figure 16.- Natural vibration modes for 45° magnesium flat-plate delta model. t/2b = 0.006.

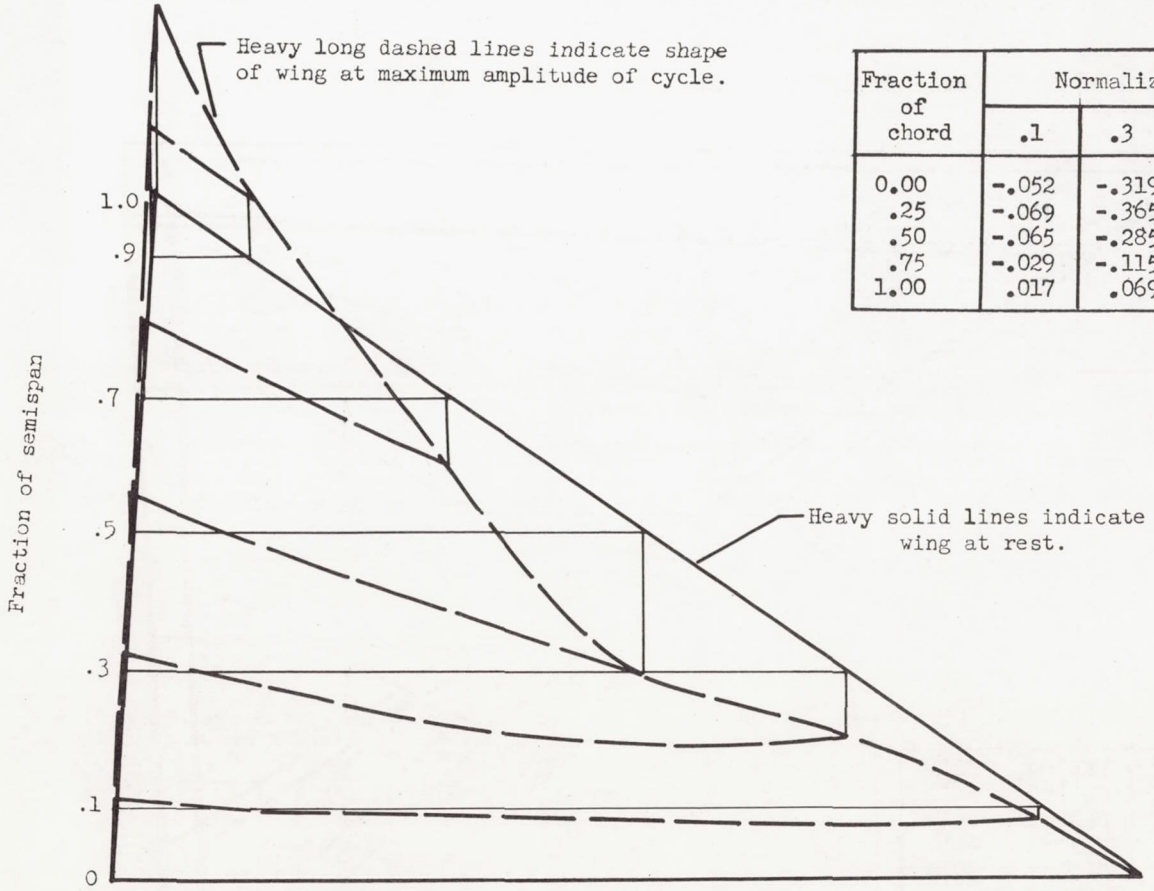

Fraction of chord	Normalized deflection at y/l =					
	.1	.3	.5	.7	.9	1.0
0.00	-.052	-.319	-.729	-.350	.325	1.0
.25	-.069	-.365	-.514	-.173	.410	1.0
.50	-.065	-.285	-.296	.020	.490	1.0
.75	-.029	-.115	-.052	.221	.580	1.0
1.00	.017	.069	.183	.420	.681	1.0

(b) Second natural vibration mode; f_2 = 184 cycles per second.

Figure 16.- Continued.

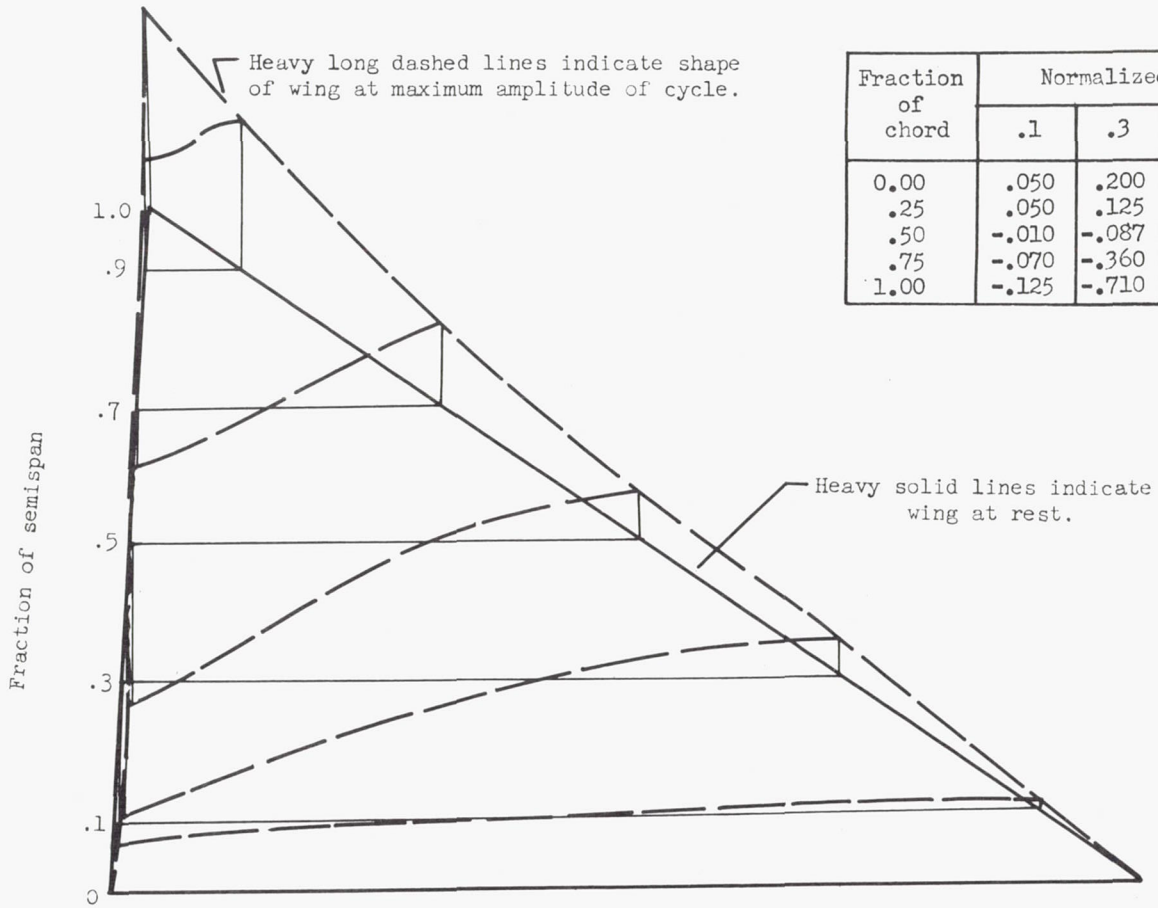

Fraction of chord	Normalized deflection at y/l =					
	.1	.3	.5	.7	.9	1.0
0.00	.050	.200	.270	.420	.760	1.0
.25	.050	.125	.130	.270	.730	1.0
.50	-.010	-.087	-.125	.075	.670	1.0
.75	-.070	-.360	-.485	-.140	.600	1.0
1.00	-.125	-.710	-.830	-.305	.575	1.0

(c) Third natural vibration mode; f_3 = 258 cycles per second.

Figure 16.- Concluded.

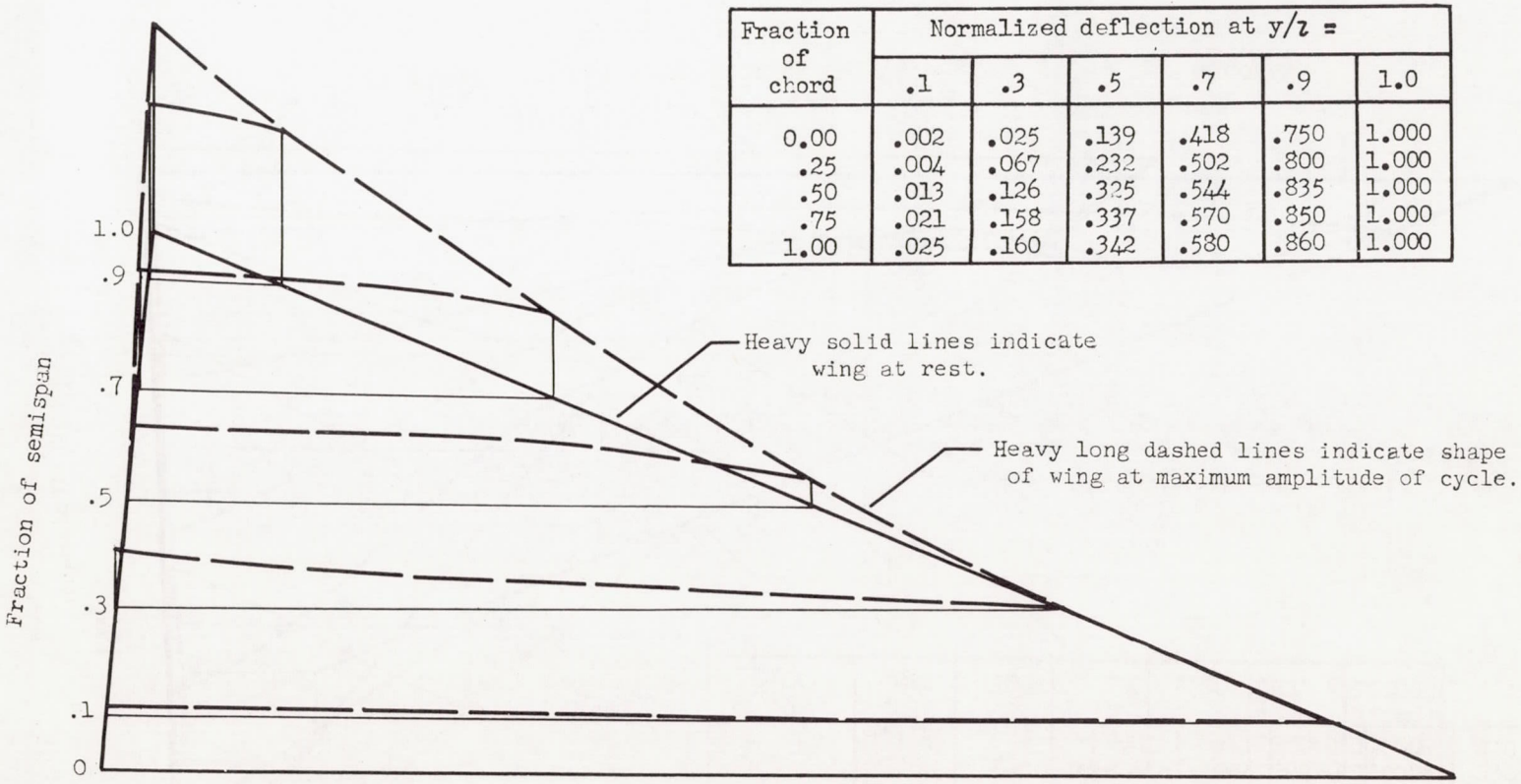

Fraction of chord	Normalized deflection at y/l =					
	.1	.3	.5	.7	.9	1.0
0.00	.002	.025	.139	.418	.750	1.000
.25	.004	.067	.232	.502	.800	1.000
.50	.013	.126	.325	.544	.835	1.000
.75	.021	.158	.337	.570	.850	1.000
1.00	.025	.160	.342	.580	.860	1.000

(a) First natural vibration mode; f_1 = 66 cycles per second.

Figure 17.- Natural vibration modes for magnesium 60° flat-plate delta model. t/2b = 0.004, based on root chord.

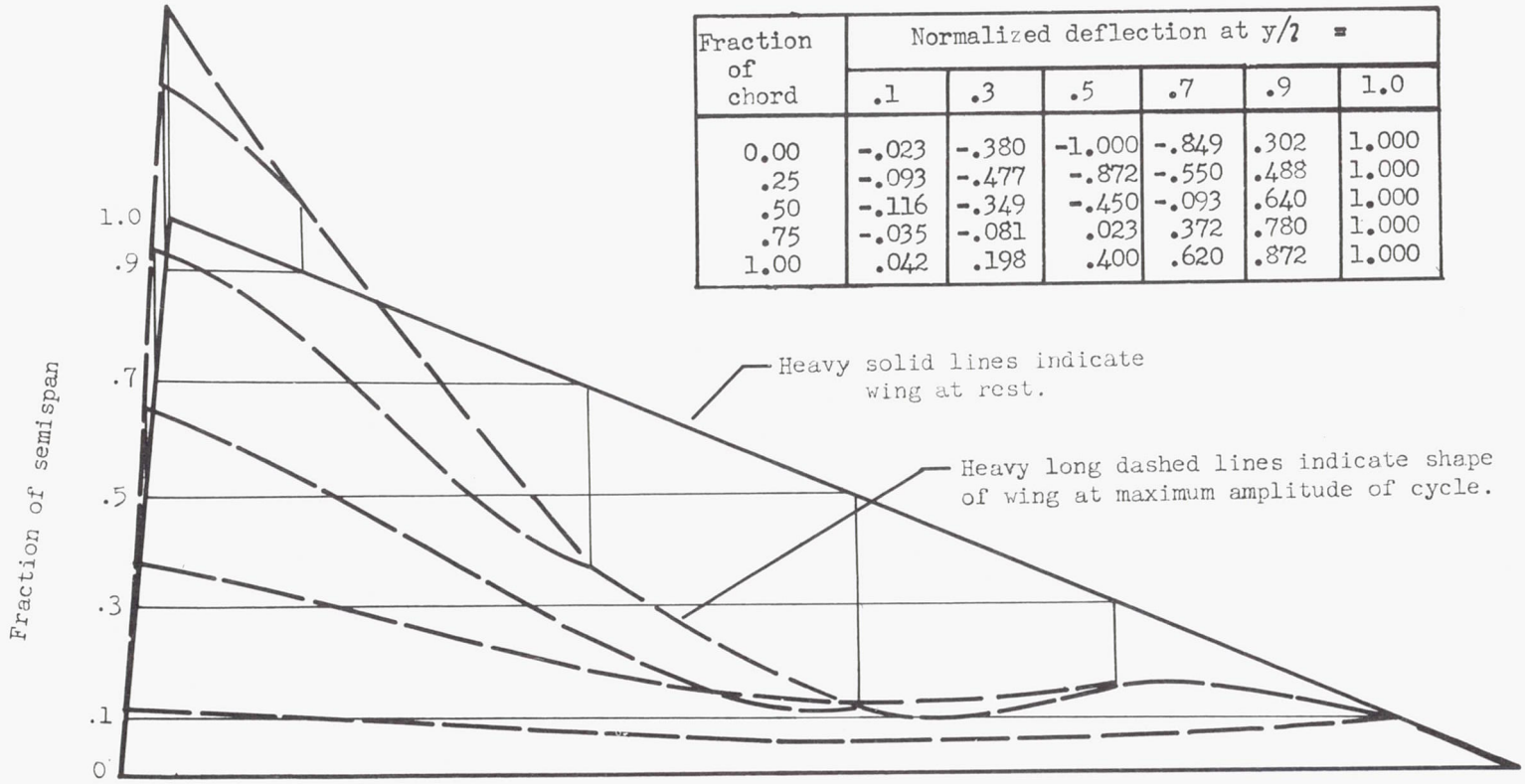

Fraction of chord	Normalized deflection at y/ℓ =					
	.1	.3	.5	.7	.9	1.0
0.00	-.023	-.380	-1.000	-.849	.302	1.000
.25	-.093	-.477	-.872	-.550	.488	1.000
.50	-.116	-.349	-.450	-.093	.640	1.000
.75	-.035	-.081	.023	.372	.780	1.000
1.00	.042	.198	.400	.620	.872	1.000

(b) Second natural vibration mode; f_2 = 185 cycles per second.

Figure 17.- Continued.

Fraction of chord	Normalized deflection at y/l =					
	.1	.3	.5	.7	.9	1.0
0.00	.006	.076	.059	.150	.745	1.000
.25	.029	.071	.029	.132	.722	1.000
.50	-.006	-.053	-.147	.070	.695	1.000
.75	-.053	-.417	-.488	-.040	.667	1.000
1.00	-.147	-.500	-.523	-.112	.640	1.000

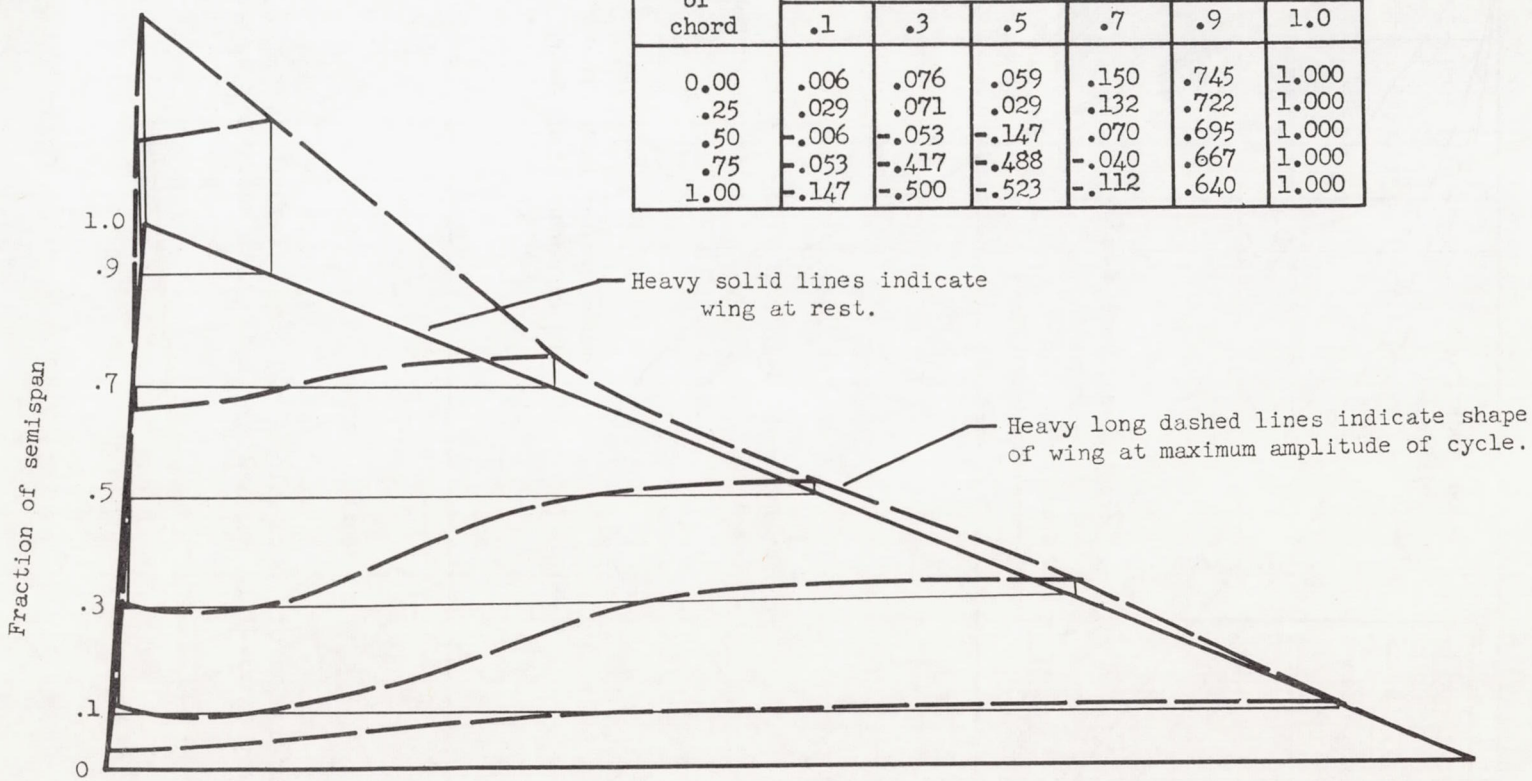

(c) Third natural vibration mode; f_3 = 336 cycles per second.

Figure 17.- Concluded.

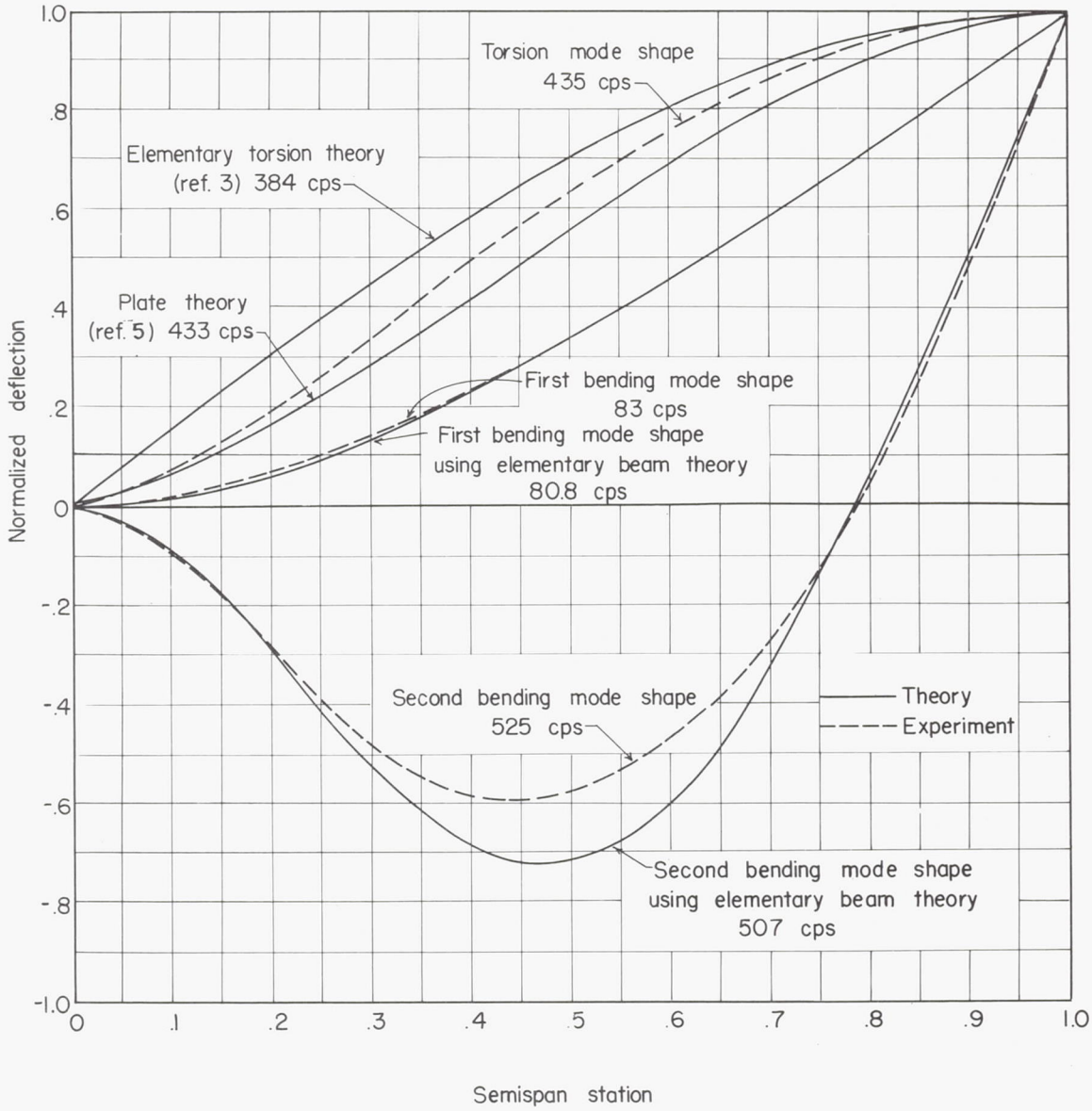

Figure 18.- Comparison of theoretical and experimental vibration modes of 2- by 5- by 0.064-inch magnesium flat-plate cantilevered-wing model.